Unraveling the $0\nu\beta\beta$ decay mechanisms

Lukáš Gráf,[1,2,3,*] Manfred Lindner,[1,†] and Oliver Scholer[1,‡]

[1]*Max-Planck-Institut für Kernphysik, Saupfercheckweg 1, 69117 Heidelberg, Germany*
[2]*Department of Physics, University of California, Berkeley, Berkeley, California 94720, USA*
[3]*Department of Physics, University of California, San Diego, La Jolla, California 92093, USA*

(Received 6 May 2022; accepted 5 July 2022; published 19 August 2022)

We discuss the possibilities of distinguishing among different mechanisms of neutrinoless double beta decay arising in the effective field theory framework. Following the review and detailed investigation of the particular ways of discrimination, we conclude that the 32 different low-energy effective operators can be split into multiple groups that are in principle distinguishable from each other by measurements of the phase-space observables and by comparison of the decay rates obtained using different isotopes. This would require not only a substantial experimental precision but necessarily also a considerable improvement of the current theoretical knowledge of the underlying nuclear physics. Specifically, the limiting aspect in our approach turns out to be the currently unknown or uncertain values of low-energy constants. Besides the study adopting the effective field theory language we also look into several typical UV models.

DOI: 10.1103/PhysRevD.106.035022

I. INTRODUCTION

The unknown origin of neutrino masses, being one of the major puzzles of contemporary particle physics, strongly motivates the quest for lepton number violation in nature. The prominent way of probing this symmetry is the search for neutrinoless double beta ($0\nu\beta\beta$) decay [1], observation of which would imply nonzero Majorana neutrino masses in accordance with the black-box theorem [2].

Besides the tight connection to neutrino masses as realized in the standard mass mechanism, neutrinoless double beta decay can be triggered in a variety of different ways, and thus potentially involve also other new physics. Generally, one can study higher-dimensional lepton-number-violating operators that can trigger $0\nu\beta\beta$ decay [3–13]. In fact, while the sole observation of $0\nu\beta\beta$ decay would indeed indicate that neutrinos acquire Majorana mass, it remains unclear whether the standard mechanism that gives a contribution proportional to the neutrino mass would be the dominant one. Examples of models beyond the standard model that can induce nonstandard contributions to the $0\nu\beta\beta$ decay rate include, for instance, the left-right symmetric models [14–17] triggering several distinct mechanisms [8,18]. Sterile neutrinos can also contribute to $0\nu\beta\beta$ decay [18–24].

There is variety of experiments searching for $0\nu\beta\beta$ decay in different double-beta-decaying isotopes [25–34]. Currently, the best limit on the half-life reaching 2.3×10^{26} years is claimed by the KamLAND-Zen collaboration [35] studying the decay of ^{136}Xe. The most stringent limit on the half-life of $0\nu\beta\beta$ decay of ^{76}Ge attains 1.8×10^{26} years, as obtained by the GERDA collaboration [25]. Proposed next generation experiments such as LEGEND [36,37] (^{76}Ge), CUPID [38] (^{100}Mo), SNO+ [39] (^{130}Te) and nEXO [40] (^{136}Xe) aim towards testing half-lives of the order of 10^{27}–10^{28} years. Some experiments like NEMO-3 are also equipped with the technology to track individual electrons and measure the individual electron energy spectra and the opening angle between the two electrons, which can help to uncover new physics not only in $0\nu\beta\beta$ decay, but even in standard double beta decay [41]. Recent reviews of the experimental and theoretical efforts in the field of $0\nu\beta\beta$ decay can be found, e.g., in Refs. [42–44].

In this work we focus on different possibilities of experimental discrimination among different mechanisms inducing $0\nu\beta\beta$ decay. To do so, we adopt the effective field theory (EFT) framework developed in Refs. [9,10], which is briefly introduced in Sec. II. In subsequent Sec. III we study the possible ways of distinguishing among the relevant set of low-energy EFT operators from $0\nu\beta\beta$ decay observables. After having discussed the single operator settings, we turn towards more complete models in Sec. IV. Finally, we summarize our findings in Sec. V. This work has been carried out utilizing the upcoming NUBB code package [45].

*lukas.graf@berkeley.edu
†lindner@mpi-hd.mpg.de
‡scholer@mpi-hd.mpg.de

II. EFT APPROACH TO $0\nu\beta\beta$ DECAY: THE MASTER FORMULA

A. The half-life master formula

As we apply in this work the effective field theory approach introduced by [9,10], let us start by briefly summarizing the most important parts. Below the scale of electroweak symmetry breaking the $0\nu\beta\beta$ decay amplitude can be described in terms of an $SU(3)_C \times U(1)_Q$ invariant low-energy effective field theory (LEFT). Including operators up to LEFT dimension 9 the most relevant Lagrangians for $0\nu\beta\beta$ are given by [9,10]

$$\begin{aligned}\mathcal{L}^{(6)}_{\Delta L=2} = \frac{2G_F}{\sqrt{2}}\Big[&C^{(6)}_{\mathrm{VL}}(\overline{u_L}\gamma^\mu d_L)(\overline{e_R}\gamma_\mu \nu^c_L) \\ &+ C^{(6)}_{\mathrm{VR}}(\overline{u_R}\gamma^\mu d_R)(\overline{e_R}\gamma_\mu \nu^c_L) + C^{(6)}_{\mathrm{SL}}(\overline{u_R} d_L)(\overline{e_L}\nu^c_L) \\ &+ C^{(6)}_{\mathrm{SR}}(\overline{u_L} d_R)(\overline{e_L}\nu^c_L) \\ &+ C^{(6)}_{\mathrm{T}}(\overline{u_L}\sigma^{\mu\nu} d_R)(\overline{e_L}\sigma_{\mu\nu}\nu^c_L)\Big] + \mathrm{H.c.}\end{aligned} \tag{1}$$

and

$$\begin{aligned}\mathcal{L}^{(7)}_{\Delta L=2} = \frac{2G_F}{\sqrt{2}v}\Big[&C^{(7)}_{\mathrm{VL}}(\overline{u_L}\gamma^\mu d_L)(\overline{e_L}\overleftrightarrow{\partial}_\mu \nu^c_L) \\ &+ C^{(7)}_{\mathrm{VR}}(\overline{u_R}\gamma^\mu d_R)(\overline{e_L}\overleftrightarrow{\partial}_\mu \nu^c_L)\Big] + \mathrm{H.c.}\end{aligned} \tag{2}$$

for the long-range part, where

$$\alpha \overleftrightarrow{\partial} \beta = \alpha(\partial\beta) - (\partial\alpha)\beta, \tag{3}$$

as well as the dimension 9 short-range Lagrangian

$$\begin{aligned}\mathcal{L}^{(9)}_{\Delta L=2} = \frac{1}{v^5}\sum_i \Big[&\Big(C^{(9)}_{i,R}(\overline{e_R}e^c_R) + C^{(9)}_{i,L}(\overline{e_L}e^c_L)\Big)\mathcal{O}_i \\ &+ C^{(9)}_i(\overline{e}\gamma_\mu\gamma_5 e^c)\mathcal{O}^\mu_i\Big]\end{aligned} \tag{4}$$

with the scalar $\mathcal{O}_i$ and vector $\mathcal{O}^\mu_i$ four-quark operators [10,46]

$$\begin{aligned}
\mathcal{O}_1 &= (\overline{u_L}^\alpha \gamma_\mu d^\alpha_L)(\overline{u_L}^\beta \gamma^\mu d^\beta_L), \\
\mathcal{O}_1{}' &= (\overline{u_R}^\alpha \gamma_\mu d^\alpha_R)(\overline{u_R}^\beta \gamma^\mu d^\beta_R), \\
\mathcal{O}_2 &= (\overline{u_R}^\alpha d^\alpha_L)(\overline{u_R}^\beta d^\beta_L), \\
\mathcal{O}_2{}' &= (\overline{u_L}^\alpha d^\alpha_R)(\overline{u_L}^\beta d^\beta_R), \\
\mathcal{O}_3 &= (\overline{u_R}^\alpha d^\beta_L)(\overline{u_R}^\beta d^\alpha_L), \\
\mathcal{O}_3{}' &= (\overline{u_L}^\alpha d^\beta_R)(\overline{u_L}^\beta d^\alpha_R), \\
\mathcal{O}_4 &= (\overline{u_L}^\alpha \gamma_\mu d^\alpha_L)(\overline{u_R}^\beta \gamma^\mu d^\beta_R), \\
\mathcal{O}_5 &= (\overline{u_L}^\alpha \gamma_\mu d^\beta_L)(\overline{u_R}^\beta \gamma^\mu d^\alpha_R), \\
\mathcal{O}^\mu_6 &= (\overline{u_L}^\alpha \gamma^\mu d^\alpha_L)(\overline{u_L}^\beta d^\beta_R), \\
\mathcal{O}^{\mu\prime}_6 &= (\overline{u_R}^\alpha \gamma^\mu d^\alpha_R)(\overline{u_R}^\beta d^\beta_L), \\
\mathcal{O}^\mu_7 &= (\overline{u_L} t^A \gamma^\mu d_L)(\overline{u_L} t^A d_R), \\
\mathcal{O}^{\mu\prime}_7 &= (\overline{u_R} t^A \gamma^\mu d_R)(\overline{u_R} t^A d_L), \\
\mathcal{O}^\mu_8 &= (\overline{u_L}^\alpha \gamma^\mu d^\alpha_L)(\overline{u_R}^\beta d^\beta_L), \\
\mathcal{O}^{\mu\prime}_8 &= (\overline{u_R}^\alpha \gamma^\mu d^\alpha_R)(\overline{u_L}^\beta d^\beta_R), \\
\mathcal{O}^\mu_9 &= (\overline{u_L} t^A \gamma^\mu d_L)(\overline{u_R} t^A d_L), \\
\mathcal{O}^{\mu\prime}_9 &= (\overline{u_R} t^A \gamma^\mu d_R)(\overline{u_L} t^A d_R).
\end{aligned} \tag{5}$$

Here α, β are color indices and the t^A are the generators of SU(3) in the fundamental representation given by the eight Gell-Mann matrices λ^A as $t^A = \frac{1}{2}\lambda^A, A = 1\ldots8$. The operators $\mathcal{O}$ and $\mathcal{O}'$ in 5 are related via parity transformation. Together with the standard mechanism of light Majorana neutrino exchange, this framework contains 32 different LEFT operators that can trigger $0\nu\beta\beta$ decay.

The transition from the quark level to the nuclear level can be achieved employing the chiral effective field theory (χEFT) [47]. The expected half-life contributed by the 32 effective operators is then captured by a "$0\nu\beta\beta$ master formula" combining the 32 LEFT Wilson coefficients, six different phase-space factors (PSFs) given in Table I and nuclear matrix elements (NMEs) summarized in Table II. At the same time, low-energy constants (LECs) that describe the nuclear interactions within χEFT enter the formula—we summarize these in Table III. The $0\nu\beta\beta$ half-life is then given in terms of different subamplitudes $\mathcal{A}_i$ as

$$\begin{aligned}(T^{0\nu}_{1/2})^{-1} = g_A^4\big[&G_{01}(|\mathcal{A}_\nu|^2 + |\mathcal{A}_R|^2) \\ &- 2(G_{01} - G_{04})\Re[\mathcal{A}^*_\nu \mathcal{A}_R] + 4G_{02}|\mathcal{A}_E|^2 \\ &+ 2G_{04}(|\mathcal{A}_{m_e}|^2 + \Re[\mathcal{A}^*_{m_e}(\mathcal{A}_\nu + \mathcal{A}_R)]) \\ &- 2G_{03}\Re[(\mathcal{A}_\nu + \mathcal{A}_R)\mathcal{A}^*_E + 2\mathcal{A}_{m_e}\mathcal{A}^*_E] \\ &+ G_{09}|\mathcal{A}_M|^2 + G_{06}\Re[(\mathcal{A}_\nu - \mathcal{A}_R)\mathcal{A}^*_M]\big].\end{aligned} \tag{6}$$

Assuming that the LEFT operators arise from the Standard Model EFT (SMEFT) operator basis, the dimension of the relevant operator at the SMEFT level can differ from the dimension of the low-energy effective operator. This is obviously the case for the LEFT dimension-3 neutrino mass operator that originates from dimension-5 Weinberg operator in SMEFT [48]. The LEFT dimension-6 and dimension-7 operators ($\mathcal{O}^{(6)}_{SL,SR,VL,VR,T}$ and $\mathcal{O}^{(7)}_{VL,VR}$) can all be generated by dimension-7 SMEFT operators. Similarly, the LEFT dimension-9 operators $\mathcal{O}^{(9)}_{1L,4L}$ can stem from dimension 7 in SMEFT at the matching scale m_W, while $\mathcal{O}^{(9)}_{5L}$ is induced by the running of $\mathcal{O}^{(9)}_{4L}$ from the matching scale m_W down to Λ_χ. The remaining LEFT

TABLE I. The different PSFs in terms of 10^{-14} y^{-1} used in our calculations.

	G_{01}	G_{02}	G_{03}	G_{04}	G_{06}	G_{09}
^{238}U	6.96	3.79	2.75	5.26	14.43	17.32
^{232}Th	2.70	0.73	0.76	1.83	6.35	7.14
^{198}Pt	1.23	0.55	0.44	0.90	2.64	3.10
^{160}Gd	1.33	1.68	0.73	1.12	2.25	3.08
^{154}Sm	0.44	0.28	0.18	0.34	0.87	1.08
^{150}Nd	8.82	40.15	7.00	8.25	9.83	18.78
^{148}Nd	1.36	2.10	0.79	1.17	2.15	3.09
^{136}Xe	1.88	4.64	1.26	1.69	2.58	4.14
^{134}Xe	0.08	0.02	0.02	0.05	0.18	0.20
^{130}Te	1.81	4.68	1.22	1.63	2.43	3.96
^{128}Te	0.07	0.02	0.02	0.05	0.17	0.19
^{124}Sn	1.13	2.42	0.72	1.01	1.62	2.51
^{116}Cd	2.06	6.51	1.46	1.89	2.59	4.47
^{110}Pd	0.58	0.95	0.34	0.50	0.89	1.30
^{100}Mo	1.89	6.80	1.36	1.75	2.25	4.06
^{96}Zr	2.42	10.43	1.81	2.26	2.68	5.15
^{82}Se	1.15	3.96	0.80	1.06	1.37	2.47
^{76}Ge	0.26	0.43	0.15	0.23	0.40	0.59

dimension-9 operators can originate from dimension-9 SMEFT operators except for $\mathcal{O}_{1L}^{(9)\prime}, \mathcal{O}_{2R,3R}^{(9)}$ and $\mathcal{O}_{2R,3R}^{(9)\ \prime}$ which arise at dimension 11 in SMEFT [46].

B. Subamplitudes

The subamplitudes $\mathcal{A}_i$ are categorized and defined via their corresponding leptonic currents. They each depend on the Wilson coefficients of different LEFT operators and can be written as

$$\begin{aligned}
\mathcal{A}_\nu &= \frac{m_{\beta\beta}}{m_e}\mathcal{M}_\nu^{(3)} + \frac{m_N}{m_e}\mathcal{M}_\nu^{(6)}(C_{\mathrm{SL}}^{(6)}, C_{\mathrm{SR}}^{(6)}, C_{\mathrm{T}}^{(6)}, C_{\mathrm{VL}}^{(7)}, C_{\mathrm{VR}}^{(7)}) \\
&\quad + \frac{m_N^2}{m_e v}\mathcal{M}_\nu^{(9)}(C_{1\mathrm{L}}^{(9)}, C_{1\mathrm{L}}^{(9)\prime}, C_{2\mathrm{L}}^{(9)}, C_{2\mathrm{L}}^{(9)\prime}, \\
&\quad C_{3\mathrm{L}}^{(9)}, C_{3\mathrm{L}}^{(9)\prime}, C_{4\mathrm{L}}^{(9)}, C_{5\mathrm{L}}^{(9)}), \\
\mathcal{A}_R &= \frac{m_N^2}{m_e v}\mathcal{M}_R^{(9)}(C_{1\mathrm{R}}^{(9)}, C_{1\mathrm{R}}^{(9)\prime}, C_{2\mathrm{R}}^{(9)}, C_{2\mathrm{R}}^{(9)\prime}, \\
&\quad C_{3\mathrm{R}}^{(9)}, C_{3\mathrm{R}}^{(9)\prime}, C_{4\mathrm{R}}^{(9)}, C_{5\mathrm{R}}^{(9)}), \\
\mathcal{A}_E &= \mathcal{M}_{E,L}^{(6)}(C_{\mathrm{VL}}^{(6)}) + \mathcal{M}_{E,R}^{(6)}(C_{\mathrm{VR}}^{(6)}), \\
\mathcal{A}_{m_e} &= \mathcal{M}_{m_e,L}^{(6)}(C_{\mathrm{VL}}^{(6)}) + \mathcal{M}_{m_e,R}^{(6)}(C_{\mathrm{VR}}^{(6)}), \\
\mathcal{A}_M &= \frac{m_N}{m_e}\mathcal{M}_M^{(6)}(C_{\mathrm{VL}}^{(6)}) + \frac{m_N^2}{m_e v}\mathcal{M}_M^{(9)}(C_6^{(9)}, C_6^{(9)\prime}, C_7^{(9)}, C_7^{(9)\prime}, \\
&\quad C_8^{(9)}, C_8^{(9)\prime}, C_9^{(9)}, C_9^{(9)\prime}).
\end{aligned} \tag{7}$$

The matrix elements $\mathcal{M}_i$ depend on the different LECs and Wilson coefficients. We explicitly state the dependency on the different Wilson coefficients within the brackets in (7). $\mathcal{A}_\nu$ depends on the matrix elements

$$\begin{aligned}
\mathcal{M}_\nu^{(3)} &= -V_{ud}^2\left(-\frac{1}{g_A^2}M_F + \mathcal{M}_{GT} + \mathcal{M}_T + 2\frac{m_\pi^2 \mathbf{g}_\nu^{\mathbf{NN}}}{g_A^2}M_{F,sd}\right), \\
\mathcal{M}_\nu^{(6)} &= V_{ud}\left(\frac{B}{m_N}(C_{SL}^{(6)} - C_{SR}^{(6)}) + \frac{m_\pi^2}{m_N v}(C_{VL}^{(7)} - C_{VR}^{(7)})\right)\mathcal{M}_{PS} \\
&\quad + V_{ud}C_{\mathrm{T}}^{(6)}\mathcal{M}_{T6},
\end{aligned} \tag{8}$$

TABLE II. NMEs used in our calculations based on the IBM2 model [12].

	M_F	M_{GT}^{AA}	M_{GT}^{AP}	M_{GT}^{PP}	M_{GT}^{MM}	M_T^{AA}	M_T^{AP}	M_T^{PP}	M_T^{MM}	M_{Fsd}	M_{GTsd}^{AA}	M_{GTsd}^{AP}	M_{GTsd}^{PP}	M_{Tsd}^{AP}	M_{Tsd}^{PP}
^{76}Ge	−0.78	6.06	−0.86	0.17	0.20	0.0	0.24	−0.06	0.04	−1.20	4.18	−1.24	0.29	−0.77	0.23
^{82}Se	−0.67	4.93	−0.71	0.14	0.17	0.0	0.24	−0.06	0.04	−1.01	3.46	−1.03	0.25	−0.73	0.22
^{96}Zr	−0.36	4.32	−0.64	0.13	0.15	0.0	−0.21	0.05	−0.04	−0.87	3.06	−0.89	0.21	0.64	−0.20
^{100}Mo	−0.51	5.55	−0.90	0.20	0.22	0.0	−0.29	0.07	−0.05	−1.28	4.48	−1.33	0.30	0.93	−0.28
^{110}Pd	−0.42	4.43	−0.76	0.17	0.18	0.0	−0.21	0.06	−0.04	−1.07	3.72	−1.11	0.25	0.79	−0.24
^{116}Cd	−0.34	3.17	−0.55	0.12	0.13	0.0	−0.12	0.04	−0.03	−0.80	2.72	−0.81	0.18	0.49	−0.16
^{124}Sn	−0.57	3.37	−0.50	0.11	0.12	0.0	0.12	−0.03	0.02	−0.82	2.56	−0.77	0.19	−0.42	0.13
^{128}Te	−0.72	4.32	−0.64	0.13	0.15	0.0	0.12	−0.04	0.03	−1.03	3.24	−0.98	0.24	−0.52	0.16
^{130}Te	−0.65	3.89	−0.57	0.12	0.14	0.0	0.14	−0.04	0.02	−0.94	2.95	−0.89	0.22	−0.47	0.15
^{134}Xe	−0.69	4.21	−0.62	0.13	0.15	0.0	0.12	−0.04	0.03	−0.97	3.07	−0.92	0.22	−0.48	0.15
^{136}Xe	−0.52	3.20	−0.45	0.09	0.11	0.0	0.12	−0.03	0.02	−0.73	2.32	−0.69	0.17	−0.36	0.12
^{148}Nd	−0.36	2.52	−0.48	0.11	0.12	0.0	−0.12	0.02	−0.02	−0.78	2.54	−0.79	0.19	0.30	−0.09
^{150}Nd	−0.51	3.75	−0.76	0.17	0.19	0.0	−0.12	0.04	−0.03	−0.74	2.46	−0.76	0.18	0.34	−0.10
^{154}Sm	−0.34	2.98	−0.52	0.11	0.13	0.0	−0.12	0.03	−0.02	−0.78	2.64	−0.79	0.19	0.39	−0.13
^{160}Gd	−0.42	4.22	−0.71	0.15	0.17	0.0	−0.21	0.05	−0.03	−1.02	3.52	−1.04	0.24	0.60	−0.19
^{198}Pt	−0.33	2.27	−0.50	0.11	0.12	0.0	−0.12	0.03	−0.02	−0.78	2.57	−0.78	0.18	0.37	−0.12
^{232}Th	−0.44	4.17	−0.76	0.17	0.18	0.0	−0.21	0.05	−0.04	−1.08	3.80	−1.11	0.25	0.69	−0.22
^{238}U	−0.52	4.96	−0.90	0.20	0.21	0.0	−0.21	0.06	−0.04	−1.29	4.51	−1.32	0.30	0.82	−0.25

TABLE III. Summary of the low-energy constants necessary to calculate the $0\nu\beta\beta$ half-life for all 32 different operators. The table is taken from [10] and restructured.

Known LECs		Unknown LECs	
g_A	1.271	$\lvert g_T'\rvert$	$\mathcal{O}(1)$
g_S	0.97 [49]	$\lvert g_T^{\pi\pi}\rvert$	$\mathcal{O}(1)$
g_M	4.7	$\lvert g_{1,6,7,8,9}^{\pi N}\rvert$	$\mathcal{O}(1)$
g_T	0.99 [49]	$\lvert g_{VL}^{\pi N}\rvert$	$\mathcal{O}(1)$
B	2.7 GeV	$\lvert g_T^{\pi N}\rvert$	$\mathcal{O}(1)$
$g_1^{\pi\pi}$	0.36 [50]	$\lvert g_{1,6,7}^{NN}\rvert$	$\mathcal{O}(1)$
$g_2^{\pi\pi}$	2.0 [50]	$\lvert g_{2,3,4,5}^{NN}\rvert$	$\mathcal{O}(16\pi^2)$
$g_3^{\pi\pi}$	−0.62 [50]	$\lvert g_{VL}^{NN}\rvert$	$\mathcal{O}(1)$
$g_4^{\pi\pi}$	−1.9 [50]	$\lvert g_T^{NN}\rvert$	$\mathcal{O}(1)$
$g_5^{\pi\pi}$	−8.0 [50]	$\lvert g_{VL,VR}^{E,m_e}\rvert$	$\mathcal{O}(1)$
g_ν^{NN}	$-92.9\ \mathrm{GeV}^{-2} \pm 50\%$ [51–53]		

and

$$\mathcal{M}_\nu^{(9)} = -\frac{1}{2m_N^2} C_{\pi\pi L}^{(9)} (M_{GT,sd}^{AP} + M_{T,sd}^{AP}) - \frac{2m_\pi^2}{g_A^2 m_N^2} C_{NNL}^{(9)} M_{F,sd}, \tag{9}$$

where $\mathcal{M}_\nu^{(3)}$ represents the contribution from the standard mass mechanism. In contrast to the traditional approach employing the nonrelativistic approximation, the EFT treatment contains also the contribution proportional to g_ν^{NN}, which parametrizes the contact-term contribution originating from the exchange of hard neutrinos [54,55]. $\mathcal{A}_R$ is given by

$$\mathcal{M}_R^{(9)} = \mathcal{M}_\nu^{(9)}|_{L\to R}, \tag{10}$$

for $\mathcal{A}_E$ the different contributions are

$$\begin{aligned}
\mathcal{M}_{E,L}^{(6)} &= -\frac{V_{ud} C_{VL}^{(6)}}{3} \left(\frac{g_V^2}{g_A^2} M_F + \frac{1}{3}(2M_{GT}^{AA} + M_T^{AA}) + \frac{6\mathbf{g_{VL}^E}}{g_A^2} M_{F,sd} \right), \\
\mathcal{M}_{E,R}^{(6)} &= -\frac{V_{ud} C_{VR}^{(6)}}{3} \left(\frac{g_V^2}{g_A^2} M_F - \frac{1}{3}(2M_{GT}^{AA} + M_T^{AA}) + \frac{6\mathbf{g_{VR}^E}}{g_A^2} M_{F,sd} \right),
\end{aligned} \tag{11}$$

$\mathcal{A}_{m_e}$ is determined by

$$\begin{aligned}
\mathcal{M}_{m_e,L}^{(6)} &= \frac{V_{ud} C_{VL}^{(6)}}{6} \left(\frac{g_V^2}{g_A^2} M_F - \frac{1}{3}(M_{GT}^{AA} - 4M_T^{AA}) - 3(M_{GT}^{AP} + M_{GT}^{PP} + M_T^{AP} + M_T^{PP}) - \frac{12\mathbf{g_{VL}^{m_e}}}{g_A^2} M_{F,sd} \right), \\
\mathcal{M}_{m_e,R}^{(6)} &= \frac{V_{ud} C_{VR}^{(6)}}{6} \left(\frac{g_V^2}{g_A^2} M_F + \frac{1}{3}(M_{GT}^{AA} - 4M_T^{AA}) + 3(M_{GT}^{AP} + M_{GT}^{PP} + M_T^{AP} + M_T^{PP}) - \frac{12\mathbf{g_{VR}^{m_e}}}{g_A^2} M_{F,sd} \right),
\end{aligned} \tag{12}$$

and finally $\mathcal{A}_M$ is given by

$$\begin{aligned}
\mathcal{M}_M^{(6)} &= V_{ud} C_{VL}^{(6)} \left[2\frac{g_A}{g_M}(M_{GT}^{MM} + M_T^{MM}) + \frac{m_\pi^2}{m_N^2} \left(-\frac{2}{g_A^2} \mathbf{g_{VL}^{NN}} M_{F,sd} + \frac{1}{2} \mathbf{g_{VL}^{\pi N}} (M_{GT,sd}^{AP} + M_{T,sd}^{AP}) \right) \right], \\
\mathcal{M}_M^{(9)} &= \frac{m_\pi^2}{m_N^2} \left[-\frac{2}{g_A^2} (\mathbf{g_6^{NN}} C_V^{(9)} + \mathbf{g_7^{NN}} \tilde{C}_V^{(9)}) M_{F,sd} + \frac{1}{2} (\mathbf{g_V^{\pi N}} C_V^{(9)} + \tilde{\mathbf{g}}_\mathbf{V}^{\boldsymbol{\pi}\mathbf{N}} \tilde{C}_V^{(9)}) (M_{GT,sd}^{AP} + M_{T,sd}^{AP}) \right].
\end{aligned} \tag{13}$$

In the above formulas we have defined the combined NMEs

$$\begin{aligned}
\mathcal{M}_{GT} &= M_{GT}^{AA} + M_{GT}^{AP} + M_{GT}^{PP} + M_{GT}^{MM}, \\
\mathcal{M}_T &= M_T^{AP} + M_T^{PP} + M_T^{MM}, \\
\mathcal{M}_{PS} &= \frac{1}{2} M_{GT}^{AP} + M_{GT}^{PP} + \frac{1}{2} M_T^{AP} + M_T^{PP}, \\
\mathcal{M}_{T6} &= 2\frac{\mathbf{g_T'} - \mathbf{g_T^{NN}}}{g_A^2} \frac{m_\pi^2}{m_N^2} M_{F,sd} - \frac{8g_T}{g_M} (M_{GT}^{MM} + M_T^{MM}) + \mathbf{g_T^{\pi N}} \frac{m_\pi^2}{4m_N^2} (M_{GT,sd}^{AP} + M_{T,sd}^{AP}) + \mathbf{g_T^{\pi\pi}} \frac{m_\pi^2}{4m_N^2} (M_{GT,sd}^{PP} + M_{T,sd}^{PP}).
\end{aligned} \tag{14}$$

The short-range dimension-9 LEFT operators contribute to the $C_{V,\pi\pi L,\pi NL,NNL}^{(9)}$ couplings that appear in the chiral Lagrangian. They are given by

$$
\begin{aligned}
C_V^{(9)} &= C_6^{(9)} + C_6^{(9)\prime} + C_8^{(9)} + C_8^{(9)\prime} \\
\tilde{C}_V^{(9)} &= C_7^{(9)} + C_7^{(9)\prime} + C_9^{(9)} + C_9^{(9)\prime} \\
C_{\pi\pi L}^{(9)} &= g_2^{\pi\pi}(C_{2L}^{(9)} + C_{2L}^{(9)\prime}) + g_3^{\pi\pi}(C_{3L}^{(9)} + C_{3L}^{(9)\prime}) - g_4^{\pi\pi} C_{4L}^{(9)} - g_5^{\pi\pi} C_{5L}^{(9)} - \frac{5}{3} g_1^{\pi\pi} m_\pi^2 (C_{1L}^{(9)} + C_{1L}^{(9)\prime}) \\
C_{\pi NL}^{(9)} &= \left(\mathbf{g_1^{\pi N}} - \frac{5}{6} g_1^{\pi\pi}\right)(C_{1L}^{(9)} + C_{1L}^{(9)\prime}) \\
C_{NNL}^{(9)} &= \mathbf{g_1^{NN}}(C_{1L}^{(9)} + C_{1L}^{(9)\prime}) + \mathbf{g_2^{NN}}(C_{2L}^{(9)} + C_{2L}^{(9)\prime}) + \mathbf{g_3^{NN}}(C_{3L}^{(9)} + C_{3L}^{(9)\prime}) + \mathbf{g_4^{NN}} C_{4L}^{(9)} + \mathbf{g_5^{NN}} C_{5L}^{(9)} \\
C_{\{\pi\pi,\pi N,NN\}R} &= C_{\{\pi\pi,\pi N,NN\}L}\big|_{L\to R}.
\end{aligned} \tag{15}
$$

The two LECs $g_V^{\pi N}$ and $\tilde{g}_V^{\pi N}$ are defined as

$$
\begin{aligned}
\mathbf{g_V^{\pi N}} &= \mathbf{g_6^{\pi N}} + \mathbf{g_8^{\pi N}} \\
\mathbf{\tilde{g}_V^{\pi N}} &= \mathbf{g_7^{\pi N}} + \mathbf{g_9^{\pi N}}.
\end{aligned} \tag{16}
$$

For the sake of convenience, we have marked all currently unknown LECs including g_ν^{NN} in **bold** within the above formulas.

In this work we will study the different LEFT operators at the matching scale of $\Lambda = m_W$ at which one would usually match the new beyond the Standard Model (BSM) physics onto LEFT. The running of the operators down to the scale of χPT at $\Lambda_\chi \simeq 2$ GeV is described in [10].

C. Relation to literature

A different basis to describe $0\nu\beta\beta$ decay developed first in [3,4] that is often used in the literature is defined by a set of 29 dimension-6 and dimension-9 lepton number violating LEFT operators given by

$$
\mathcal{L}_6 = \frac{G_F}{\sqrt{2}} \sum_{i,k} \epsilon_k^i j_i J_k \tag{17}
$$

for the long-range part with $i,k \in \{V\pm A, S\pm P, T_L, T_R,\}$ and

$$
\begin{aligned}
\mathcal{L}_9 = \frac{G_F^2}{2m_N} \sum_{l,m,n} [&\epsilon_1^{lmn} J_l J_m j_n + \epsilon_2^{lmn} J_l^{\mu\nu} J_{\mu\nu_m} j_n \\
&+ \epsilon_3^{lmn} J_l^\mu J_{\mu_m} j_n + \epsilon_4^{lmn} J_l^\mu J_{\mu\nu_m} j_n^\nu + \epsilon_5^{lmn} J_l^\mu J_m j_{\mu n}]
\end{aligned} \tag{18}
$$

for the short-range part with $l,m,n \in \{L,R\}$. Here, ϵ_k^i and ϵ^{lmn} are the Wilson coefficients of the different long- and short-range operators. The quark currents J are given by[1]

$$
\begin{aligned}
J_{S\pm P} &= J_{R,L} = \bar{u}(1\pm\gamma_5)d, \\
J_{V\pm A} &= J_{R,L}^\mu = \bar{u}\gamma^\mu(1\pm\gamma_5)d, \\
J_{T_{R,L}} &= J_{R,L}^{\mu\nu} = \bar{u}\sigma^{\mu\nu}(1\pm\gamma_5)d,
\end{aligned} \tag{19}
$$

[1]We keep the two different types of indices for the short-range currents to stick with the literature.

and the lepton currents j are given by

$$
\begin{aligned}
j_{S\pm P} &= \bar{e}(1\pm\gamma_5)\nu^c, \qquad j_{V\pm A} = \bar{e}\gamma^\mu(1\pm\gamma_5)\nu^c \\
j_{T_{R,L}} &= \bar{e}\sigma^{\mu\nu}(1\pm\gamma_5)\nu^c, \qquad j_{R,L} = \bar{e}(1\pm\gamma_5)e^c \\
j_{R,L}^\mu &= \bar{e}\gamma^\mu(1\pm\gamma_5)e^c.
\end{aligned} \tag{20}
$$

This framework does not include the dimension-7 operators of the framework utilized in our approach. While the remaining long-range part of the two descriptions can be related easily, the short-range operators are related to each other via Fierz transformations. One finds that

$$
\begin{aligned}
C_{1L}^{(9)} &= \frac{2v}{m_N}\epsilon_3^{LLL}, \qquad C_{1L}^{(9)\prime} = \frac{2v}{m_N}\epsilon_3^{RRL}, \\
C_{1R}^{(9)} &= \frac{2v}{m_N}\epsilon_3^{LLR}, \qquad C_{1R}^{(9)\prime} = \frac{2v}{m_N}\epsilon_3^{RRR}, \\
C_{2L}^{(9)} &= \frac{2v}{m_N}(\epsilon_1^{LLL} - 4\epsilon_2^{LLL}), \\
C_{2L}^{(9)\prime} &= \frac{2v}{m_N}(\epsilon_1^{RRL} - 4\epsilon_2^{RRL}), \\
C_{2R}^{(9)} &= \frac{2v}{m_N}(\epsilon_1^{LLR} - 4\epsilon_2^{LLR}), \\
C_{2R}^{(9)\prime} &= \frac{2v}{m_N}(\epsilon_1^{RRR} - 4\epsilon_2^{RRR}), \\
C_{3L}^{(9)} &= -\frac{16v}{m_N}\epsilon_2^{LLL}, \qquad C_{3L}^{(9)\prime} = -\frac{16v}{m_N}\epsilon_2^{RRL}, \\
C_{3R}^{(9)} &= -\frac{16v}{m_N}\epsilon_2^{LLR}, \qquad C_{3R}^{(9)\prime} = -\frac{16v}{m_N}\epsilon_2^{RRR}, \\
C_{4L}^{(9)} &= \frac{2v}{m_N}\epsilon_3^{RLL}, \qquad C_{4R}^{(9)} = \frac{2v}{m_N}\epsilon_3^{RLR}, \\
C_{5L}^{(9)} &= -\frac{v}{m_N}\epsilon_1^{RLL}, \qquad C_{5R}^{(9)} = -\frac{v}{m_N}\epsilon_1^{RLR}, \\
C_6^{(9)} &= \frac{v}{m_N}\left(\epsilon_5^{LRR} + i\frac{5}{3}\epsilon_4^{LRR}\right), \\
C_6^{(9)\prime} &= \frac{v}{m_N}\left(\epsilon_5^{RLR} + i\frac{5}{3}\epsilon_4^{RLR}\right),
\end{aligned}
$$

$$C_7^{(9)} = 4i\frac{v}{m_N}\epsilon_4^{LRR}, \qquad C_7^{(9)\prime} = 4i\frac{v}{m_N}\epsilon_4^{RLR},$$
$$C_8^{(9)} = \frac{v}{m_N}\left(\epsilon_5^{LLR} - i\frac{5}{3}\epsilon_4^{LLR}\right),$$
$$C_8^{(9)\prime} = \frac{v}{m_N}\left(\epsilon_5^{RRR} - i\frac{5}{3}\epsilon_4^{RRR}\right),$$
$$C_9^{(9)} = -4i\frac{v}{m_N}\epsilon_4^{LLR}, \quad C_9^{(9)\prime} = -4i\frac{v}{m_N}\epsilon_4^{RRR}. \tag{21}$$

The main difference between the two set of operators is that the ϵ basis contains short-range tensor operators instead of color octets.

III. DISTINGUISHING THE EFFECTIVE OPERATORS

Neutrinoless double-β-decay, if observed, would be characterized by several experimental observables, precise determination of which can give us some insight into the underlying BSM physics. Generally, the $0\nu\beta\beta$ decay experiments can be able to determine decay rate, single electron energy spectrum and angular correlation between the two emitted electrons. Additional information might be obtained by studying different $\beta\beta$ modes or by employing complementary information from other experiments such as the LHC [56,57]. In the following, we will discuss possible ways of experimentally distinguishing among the 32 different $0\nu\beta\beta$ decay inducing LEFT operators with a focus on the limiting factors of a potential confirmation/exclusion of the existence of any additional nonstandard scenario contributing to $0\nu\beta\beta$ decay alongside the standard mass mechanism.

A. Phase-space observables

While most experimental collaborations only attempt to measure the half-life of $0\nu\beta\beta$ decay, some experiments like NEMO-3 [58], or its future successor SuperNEMO [59], are designed to also measure the single electron energy spectrum and the angular correlation of the two outgoing electrons. These are associated with different electron currents and within the simplest approximation they can be calculated analytically. More exact solutions require numeric calculations of the exact electron wave functions [60]. The different PSFs G_{0k} can be written in the form [61]

$$G_{0k} = \frac{(G_F V_{ud})^4 m_e^2}{64\pi^5 \ln 2 R^2}\int \delta(\epsilon_1+\epsilon_2+E_f-E_i) \times (h_{0k}(\epsilon_1,\epsilon_2,R)\cos\theta + g_{0k}(\epsilon_1,\epsilon_2,R)) \times p_1 p_2 \epsilon_1 \epsilon_2 \mathrm{d}\epsilon_1 \mathrm{d}\epsilon_2 \mathrm{d}(\cos\theta), \tag{22}$$

where $p_{1,2}$ and $\epsilon_{1,2}$ are the momentum and energy of the first and second released electron, R is the radius of the final-state nucleus and $E_{i,f}$ denotes the energy of the initial- or final-state nucleus, respectively. Here, we denote the part of the differential phase-space factor independent of the angle between the two outgoing electrons as g_{0k}, while h_{0k} is the angular correlation part proportional to the cosine of the opening angle θ. Additionally, $G_{04,06,09}$ have to be rescaled to comply with the definitions in [9,10] as

$$G_{04} \to \frac{9}{2}G_{04}, \quad G_{06} \to \frac{m_e R}{2}G_{06}, \quad G_{09} \to \left(\frac{m_e R}{2}\right)^2 G_{09}. \tag{23}$$

The relations between the electron wave functions and the functions h_{0k} and g_{0k} are given in [61] to which we will refer here. We apply their simplest approximation scheme "A" assuming a uniform charge distribution in the nucleus. Using Eq. (22) one can write the angular correlation coefficient a_1/a_0 which is defined via

$$\frac{\mathrm{d}\Gamma}{\mathrm{d}\cos\theta \mathrm{d}\tilde{\epsilon}_1} = a_0\left(1+\frac{a_1}{a_0}\cos\theta\right) \tag{24}$$

with

$$\tilde{\epsilon}_i = \frac{\epsilon_i - m_e}{Q_{\beta\beta}} \in [0,1] \tag{25}$$

as

$$\frac{a_1}{a_0}(\tilde{\epsilon}) = \frac{\sum_i |M_i|^2 h_{0i}(\epsilon, \Delta M_{\mathrm{Nuclei}} - \epsilon, R)}{\sum_j |M_j|^2 g_{0j}(\epsilon, \Delta M_{\mathrm{Nuclei}} - \epsilon, R)}. \tag{26}$$

Here, $\Delta M_{\mathrm{Nuclei}}$ is the mass difference between the mother and daughter nuclei and $Q_{\beta\beta}$ denotes the Q value of the decay. The potential of utilizing the angular correlation of the outgoing electrons for discrimination between different mechanisms of $0\nu\beta\beta$ has been discussed, e.g., in [62]. Similarly, the single electron spectra are given by

$$\frac{\mathrm{d}\Gamma}{\mathrm{d}\epsilon_1} = \frac{(G_F V_{ud})^4 m_e^2}{64\pi^5 \ln 2 R^2}\left(\sum_i |M_i|^2 g_{0i}(\epsilon, \Delta M_{\mathrm{Nuclei}} - \epsilon, R)\right) \times p_1 p_2 \epsilon(\Delta M_{\mathrm{Nuclei}} - \epsilon). \tag{27}$$

Consequently, approximating the electron wave functions, we can easily calculate the expected angular correlation factor and single electron spectra for each of the 32 LEFT operators. The normalized single electron spectra as well as the angular correlations corresponding to each of the six distinct PSFs are shown in Fig. 1. As we can see, using these observables the operators associated with distinct PSFs are in principle distinguishable from each other, provided substantial experimental accuracy is reached.

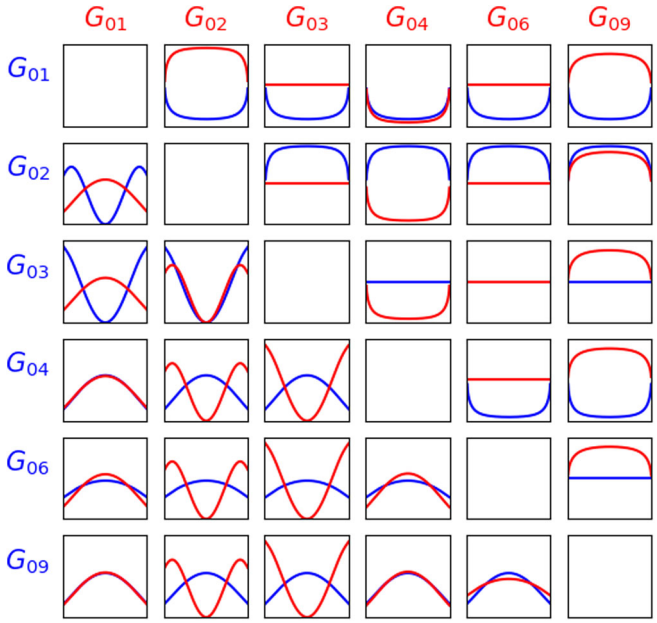

FIG. 1. Comparison of the normalized single electron spectra (lower left) and angular correlation coefficients (upper right) in ^{136}Xe that result from the six PSFs which appear in the $0\nu\beta\beta$ half-life "master formula." Red curves correspond to the red-labeled PSFs on the horizontal axis, while blue curves represent the PSFs denoted in blue on the vertical axis. The x axis covers the range $\tilde{\epsilon} \in [0\text{–}1]$.

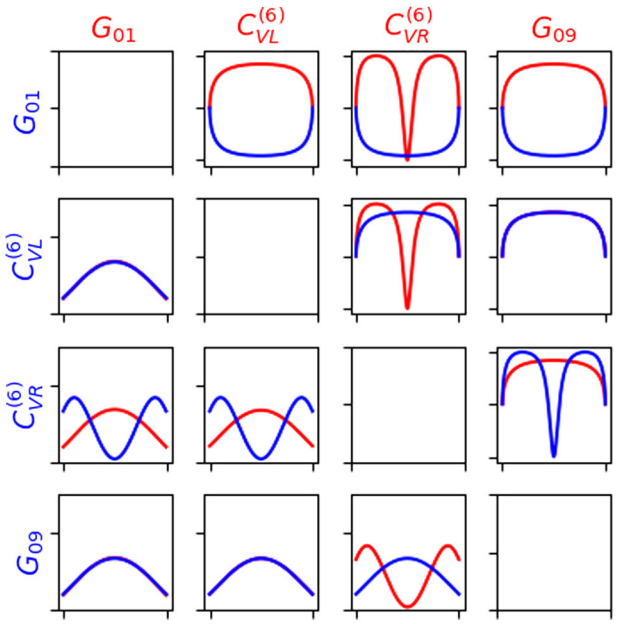

FIG. 2. Normalized single electron spectra (lower left) and angular correlation coefficients (upper right) for each of the four distinguishable groups of operators. The shapes are shown for ^{136}Xe assuming the naive dimensional analysis (NDA) values for the currently unknown LECs. However, the particular choice does not result in a significant difference in the general shape of the plots. Red curves correspond to the red-labeled operator group on the horizontal axis, while blue curves represent the operator group denoted in blue on the vertical axis. The x axis covers the range $\tilde{\epsilon} \in [0-1]$.

However, distinguishing among different $0\nu\beta\beta$ mechanisms purely based on the phase-space observables has its obvious limitations. In fact, while G_{06} is only induced in the presence of multiple operators the dimension-6 vector operators both trigger several of the remaining PSFs. Taking this into account, we can identify four different groups of operators that are in principle distinguishable using the leptonic PSF observables, namely: $C_{VL}^{(6)}, C_{VR}^{(6)}$, the operators corresponding to G_{01} and the ones corresponding to G_{09}. The PSF observables that result from each of these four groups are shown in Fig. 2. Here, we can see that the left-handed vector current operator $C_{VL}^{(6)}$ and the operators corresponding to G_{09}, while corresponding to distinct PSFs, are practically indistinguishable since the $C_{VL}^{(6)}$ phase space turns out to be dominated by the contribution from G_{09}. The remaining groups are distinguishable from each other using at least one of the considered observables.

Note that while the electron wave functions depend on the charge of the daughter nucleus as well as on the decay energy, the general shape of the induced observables is not very dependent on the choice of the decaying isotope. In Fig. 3 we show the single electron spectra and in Fig. 4 the angular correlation coefficients corresponding to the six different PSFs in four different naturally occurring $0\nu\beta^-\beta^-$ isotopes.

B. Decay rate ratios

The remaining $0\nu\beta\beta$ observable is the decay rate Γ itself. While the phase space can be used to distinguish operators with different leptonic currents, information about the decay rates in various isotopes can be also applied to operators with distinct hadronic structures, as these give rise to different NMEs. The isotope dependence of the existing calculations of NMEs can be inferred from Table II. Therefore, one can study the half-life ratios,

$$R^{\mathcal{O}_i}(^{\mathrm{A}}\mathrm{X}) \equiv \frac{T_{1/2}^{\mathcal{O}_i}(^{\mathrm{A}}\mathrm{X})}{T_{1/2}^{\mathcal{O}_i}(^{76}\mathrm{Ge})} = \frac{\sum_j |\mathcal{M}_j^{\mathcal{O}_i}(^{76}\mathrm{Ge})|^2 G_j^{\mathcal{O}_i}(^{76}\mathrm{Ge})}{\sum_k |\mathcal{M}_k^{\mathcal{O}_i}(^{\mathrm{A}}\mathrm{X})|^2 G_k^{\mathcal{O}_i}(^{\mathrm{A}}\mathrm{X})}, \tag{28}$$

where $T_{1/2}^{\mathcal{O}_i}(^{A}X)$ is the half-life induced by the operator O_i in the isotope ^{A}X. The sums $\sum_{j,k}$ are taken over all different PSFs generated by the operator $\mathcal{O}_i$ and become relevant only for $C_{VL,VR}^{(6)}$ [see Eqs. (B2) and (B3)]. Studying the half-life ratio allows for elimination of the unknown particle physics couplings, as was first discussed in [63] and shortly after also in [64]. Here, we take ^{76}Ge for the reference isotope. To be able to quantify how well one can distinguish two different operators $\mathcal{O}_{i,j}$ from each other we can take the ratio

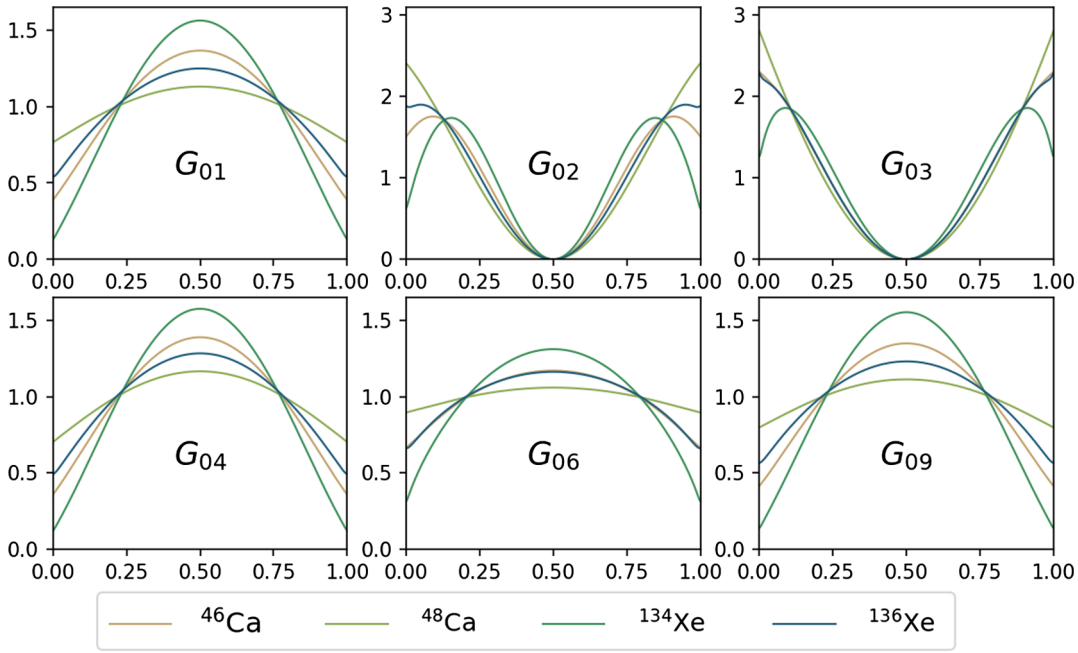

FIG. 3. The single electron spectra for four different naturally occurring $0\nu\beta^-\beta^-$ isotopes are shown. While the exact quantitative curves depend on the choice of the isotope, their shape is mostly independent of this choice. As before, the x axis shows the normalized electron energy $\tilde{\epsilon}$.

$$R_{ij}({}^{A}X) = \frac{R^{\mathcal{O}_i}({}^{A}X)}{R^{\mathcal{O}_j}({}^{A}X)}. \tag{29}$$

Specifically, the ratios $R_{im_{\beta\beta}}$ relating the nonstandard mechanisms with the standard mass mechanism will be of interest to compare the effect of different higher-dimensional operators and possibly identify the existence of additional exotic contributions to the $0\nu\beta\beta$ rate in experiments. Obviously, two operators $\mathcal{O}_{i,j}$ would be indistinguishable via this method if the resulting ratio would equal unity, i.e., if $R_{ij} = 1$. Vice versa, they would be perfectly distinguishable for either $R_{ij} \to \infty$ or $R_{ij} = 0$, that is, for $|\log_{10}(R_{ij})| \to \infty$.

Studying the decay rate ratios has several benefits. First of all, in case only one Wilson coefficient contributes at a

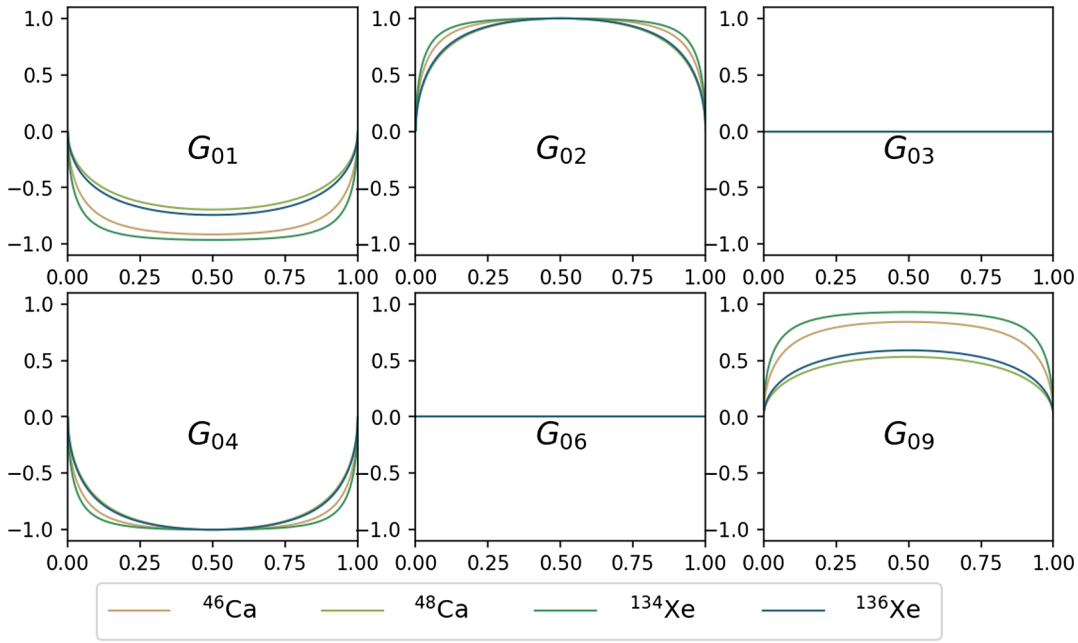

FIG. 4. Comparison of the angular correlation coefficients in four different isotopes as done for the single electron energy spectra in Fig. 3.

TABLE IV. Operator groups that can possibly be distinguished via taking decay rate ratios. The choice of the groups depends on the knowledge of the LECs. If we set the unknown LECs to zero, the short-range scalar operator groups $C^{(9)}_{S2-S5}$ become indistinguishable as well as the short-range vector operator groups $\tilde{C}^{(9)}_V$ and $\tilde{C}^{(9)}_V$. Improved knowledge of the LECs, assuming no fine-tuning, would allow to distinguish among these operator groups.

$m_{\beta\beta}$	$C^{(6)}_{VL}$	$C^{(6)}_{VR}$	$C^{(6)}_{T}$	$C^{(6,7)}_{S,V}$	$C^{(9)}_{S1}$	$C^{(9)}_{S2}$	$C^{(9)}_{S3}$	$C^{(9)}_{S4}$	$C^{(9)}_{S5}$	$C^{(9)}_{V}$	$\tilde{C}^{(9)}_{V}$
$m_{\beta\beta}$	$C^{(6)}_{VL}$	$C^{(6)}_{VR}$	$C^{(6)}_{T}$	$C^{(6)}_{SL}$	$C^{(9)}_{1L}$	$C^{(9)}_{2L}$	$C^{(9)}_{3L}$	$C^{(9)}_{4L}$	$C^{(9)}_{5L}$	$C^{(9)}_{6}$	$C^{(9)}_{7}$
...	...	...	...	$C^{(6)}_{SR}$	$C^{(9)}_{1R}$	$C^{(9)}_{2R}$	$C^{(9)}_{3R}$	$C^{(9)}_{4R}$	$C^{(9)}_{5R}$	$C^{(9)\prime}_{6}$	$C^{(9)\prime}_{7}$
...	...	...	...	$C^{(7)}_{VL}$	$C^{(9)\prime}_{1L}$	$C^{(9)\prime}_{2L}$	$C^{(9)\prime}_{3L}$	...	...	$C^{(9)}_{8}$	$C^{(9)}_{9}$
...	...	...	...	$C^{(7)}_{VR}$	$C^{(9)\prime}_{1R}$	$C^{(9)\prime}_{2R}$	$C^{(9)\prime}_{3R}$	...	...	$C^{(9)\prime}_{8}$	$C^{(9)\prime}_{9}$

time, it drops out. Therefore, the ratio corresponding to a certain operator and its Wilson coefficient is a constant that depends only on the corresponding NMEs, LECs and PSFs. If more Wilson coefficients contribute at the same time, then only the overall magnitude can be factored out. In this case, the relations between different coefficients can, of course, affect the resulting ratios. However, one can still utilize this method to study specific models and see if they are distinguishable from the standard mass mechanism. We will discuss this possibility in Sec. IV. Additionally, when taking ratios of the half-lives, one can expect that the impact of correlated systematic relative errors on the NMEs decreases as they should (at least partially) cancel. In [65] it was shown that for the NME calculations using quasiparticle random phase approximation (QRPA) uncertainties arising from unknown g_A quenching and nucleon-nucleon potentials are correlated among different isotopes. Half-life measurements in different isotopes as a tool to discriminate among different mechanisms of $0\nu\beta\beta$ decay have also been employed previously in [66–69].

Applying this approach to the master-formula framework one can identify 12 different groups of operators that can in principle be distinguished from each other. These groups are summarized in Table IV. However, the distinguishability of the short-range operators strongly depends on the currently unknown LECs. Taking the most of the unknown LECs to be zero while keeping $g^{NN}_{6,7} = g^{\pi N}_V = \tilde{g}^{\pi N}_V = 1$ (so that the contribution from the short-range vector operators is not omitted) makes it impossible to distinguish the short-range scalar operators $C^{(9)}_{S2-S5}$ as well as the short-range vector operator groups $C^{(9)}_V$ and $\tilde{C}^{(9)}_V$.

1. Sensitivity on the unknown LECs

In Fig. 5 we present the expected ratios $R^{\mathcal{O}_i}$ as well as the normalized ratios $R_{im_{\beta\beta}}$ defined in (28) and (29) for the above choice of LECs which will be our benchmark scenario. The ratios for the ϵ *basis* are shown in Fig. 6. Additionally, to study the uncertainties arising from the unknown LECs, the plots include 1000 points per operator group that each represent variations of the unknown LECs g_i within the ranges $[-\sqrt{10}, -1/\sqrt{10}] \times |g_i|$ and $[1/\sqrt{10}, \sqrt{10}] \times |g_i|$, i.e., we vary the LECs within the range of values given by their expected order of magnitude shown in Table III. For g^{NN}_ν which generates a short-range component into the standard mass mechanism we take a variation of $\pm 50\%$. The central values of the variation, i.e., the median values, are marked by crosses.

From the upper panel of Fig. 5 one can infer that the half-life ratios $R^{m_{\beta\beta}}$ corresponding to the standard mass mechanism are not very sensitive to g^{NN}_ν (they are actually too small to be visible). In Fig. 7 we explicitly show the impact of varying the g^{NN}_ν LEC on the expected half-life in ^{76}Ge for the standard mechanism. Again, compared to the impact of the unknown Majorana phases the effect of g^{NN}_ν is minor. However, it is important to note that the impact of g^{NN}_ν on the overall magnitude of the half-life cannot be ignored as easily. For comparison, we also present the case where $g^{NN}_\nu = 0$ in Fig. 7.

For the remaining nonstandard operators, however, we can see from Fig. 5 that the values of the currently unknown LECs can have quite a significant impact on the expected ratios. Often, especially for the short-range $C^{(9)}_i$ groups, the central values are significantly offset from our benchmark scenario with most unknown LECs turned off. Hence, for these operators the appearance of the unknown LECs has a significant impact on the corresponding $0\nu\beta\beta$-decay rate. Although for some operator groups, such as $C^{(9)}_{2S-5S}$, the spread of the values of the ratios obtained by varying the unknown LECs is relatively small, for other groups like the short-range vector contributions $C^{(9)}_V, \tilde{C}^{(9)}_V$ the variation of the unknown LECs results in a significant stretch around the central values. For these ratios the precise numerical value of the unknown LECs is of particular importance. The different sensitivities of the short-range scalar and vector operators arise from the fact that for the scalar operators some of the relevant LECs, namely those encoding pion-pion interactions $g^{\pi\pi}_i$, are known, while for the short-range vector operators all relevant LECs are unknown. Since we do not fix the sign of the unknown LECs (except g^{NN}_ν) there can be a gap within the

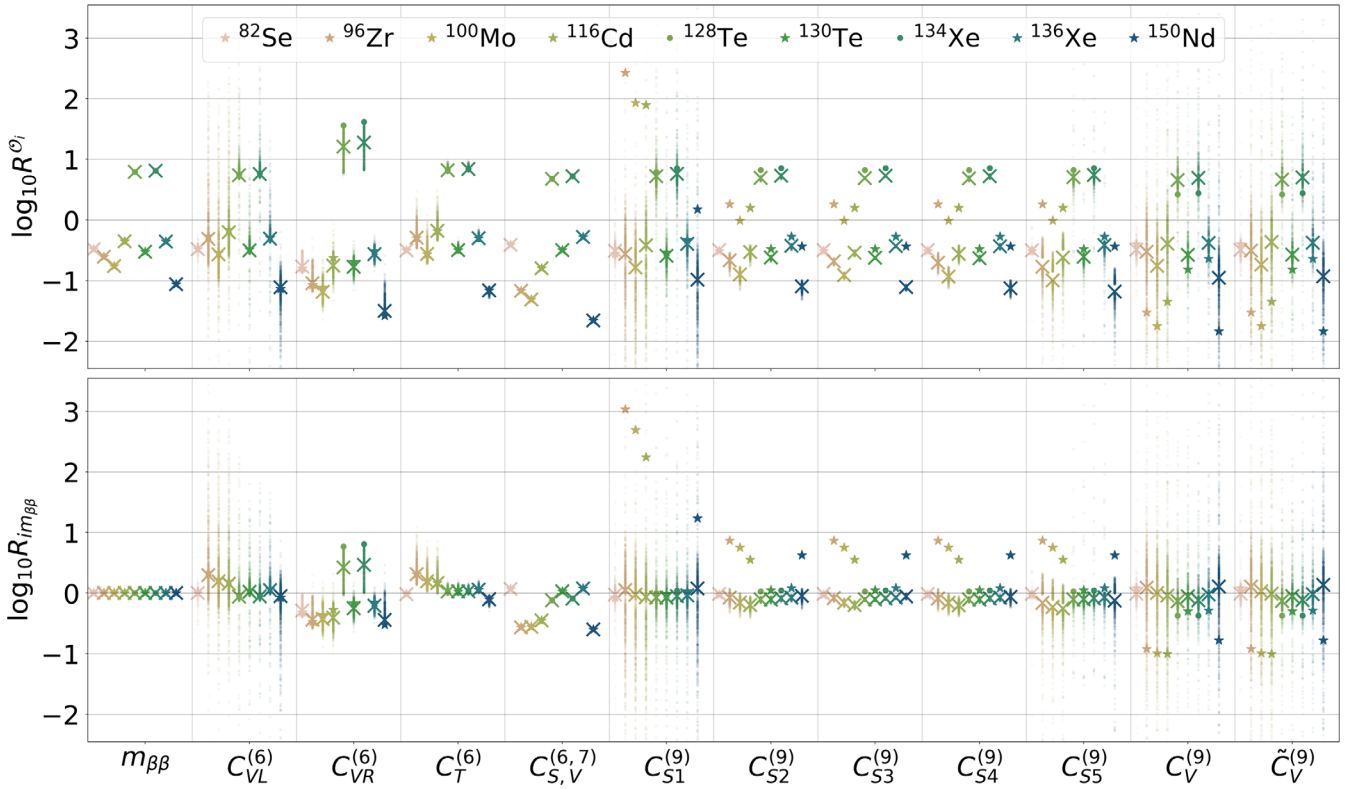

FIG. 5. The decay rate ratios R^{O_i} (upper plot) and $R_{im_{\beta\beta}}$ (lower plot) for the different operator groups are shown. The larger markers represent the choice of vanishing unknown LECs with $g_{6,7}^{NN} = g_V^{\pi N} = \tilde{g}_V^{\pi N} = 1$. Isotopes with a PSF $G_0 > 10^{-14}$ y^{-1} are represented by stars while isotopes with smaller PSFs are represented by round markers. The additional points represent variations of the different unknown LECs g_i randomly chosen from $[-\sqrt{10}, -1/\sqrt{10}] \times |g_i|$ and $[+1/\sqrt{10}, +\sqrt{10}] \times |g_i|$ except for g_ν^{NN} which is varied in a range of $\pm 50\%$. The crosses represent the central values of the variation, i.e., the median values. The reference isotope is chosen to be ^{76}Ge. Note that the variation of g_ν^{NN} does induce a small variation of $R^{m_{\beta\beta}}$ which is, however, not visible in the above plot.

LEC-varied ratios resulting in two visible central values for the operator groups, for which the ratios are sensitive to the sign of the LECs. The lower part of Fig. 5 which displays the normalized $R_{im_{\beta\beta}}$ shows that the central values of the LEC-varied ratios are closer to 0 than the benchmark scenario. Therefore, the inclusion of the unknown LECs tends to impair the distinguishability from the standard mechanism.

The above discussion clearly shows the importance of determining the yet unknown LECs involved in the calculation. This can be achieved, for example, by lattice QCD calculations [50,70,71].

2. Distinguishing different operators

When studying the $0\nu\beta\beta$ decay rate the basic question to ask is whether and how well could a nonstandard contribution be distinguished from the standard light-neutrino exchange. Employing the half-life measurements in different isotopes, one can try to identify those that are most suitable for discrimination between the mass mechanism and an exotic $0\nu\beta\beta$ decay contribution triggered by a particular higher-dimensional operator. In the first row of Fig. 8 we show the maximal ratios $R_{im_{\beta\beta}}^{\max}$ and the corresponding pair of isotopes obtained for each operator group. Here, we consider a "representative" scenario by studying the central values defined as the median ratio $R_{im_{\beta\beta}}$ of the range of values obtained from the variation of the LECs. At the same time, we identify the "worst-case scenario" ratio defined as the value within the range that is closest to unity, see the first column of Fig. 8. In this context we consider only isotopes with existing experimental limits on the half-life, namely, the following: ^{76}Ge [25], ^{82}Se [26], ^{96}Zr [27], ^{100}Mo [28], ^{116}Cd [29], ^{128}Te [30], ^{130}Te [31], ^{134}Xe [72], ^{136}Xe [33] and ^{150}Nd [34]. Figure 8 also presents all the other ratios $R_{ij}^{\max}$ quantifying the mutual distinguishability of all the operator groups with the values corresponding to the representative scenario above the diagonal and the worst-case scenario below the diagonal. In addition, the dashed lines in Fig. 8 mark the pairs of operators that could be discriminated using the phase-space observables.

Considering the central values, the nonstandard long-range operators $C_{VR}^{(6)}$ and $C_{S,V}^{(6,7)}$ give the most distinct half-life ratios compared to the standard mass mechanism while the remaining long-range operator groups $C_{VL}^{(6)}$ and $C_T^{(6)}$

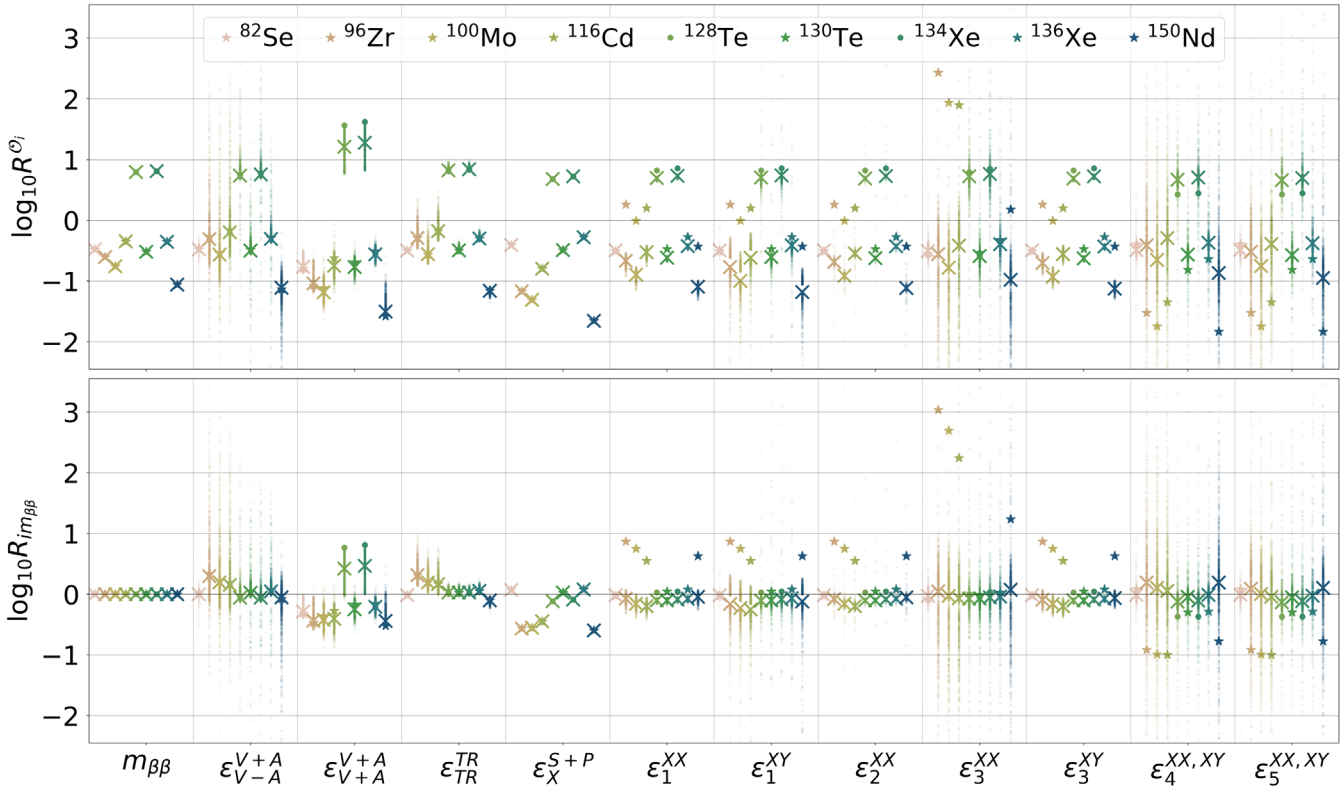

FIG. 6. The decay rate ratios R^{O_i} (upper plot) and $R_{im_{\beta\beta}}$ (lower plot) for the different operator groups in the ϵ basis similar to Fig. 5 are shown.

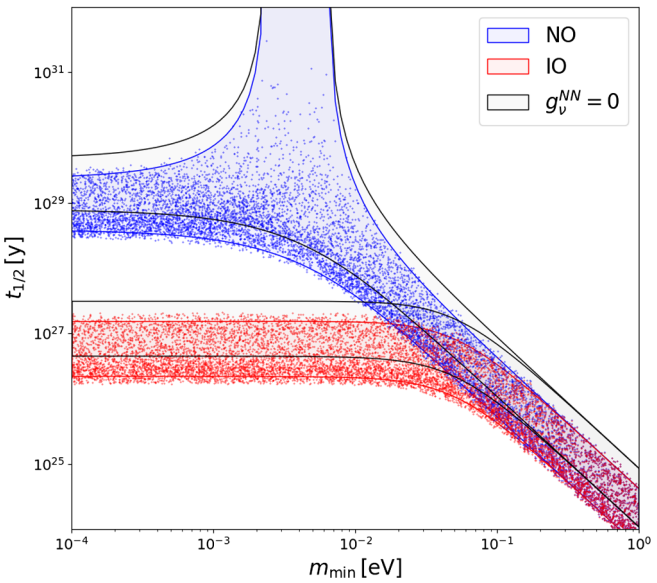

FIG. 7. Here we show the half-life for ^{76}Ge in dependence on the minimal neutrino mass $m_{\min}$ for both normal (NO) and inverted (IO) neutrino mass ordering. The scatter points were obtained by marginalizing over g_ν^{NN} and the unknown Majorana phases. The blue and red contours show the possible half-life ranges when only the phases are varied, while g_ν^{NN} is fixed. Additionally, the black contours correspond to $g_\nu^{NN}=0$.

also result in sizable $R^{\max}_{im_{\beta\beta}} > 2$. Additionally, both $C^{(6)}_{VL}$ and $C^{(6)}_{VR}$ could be identified by measuring the angular correlation of the emitted electrons. The nonstandard short-range operators generally tend to have lower values of the ratios $R^{\max}_{im_{\beta\beta}} < 2$; thus, there is less potential for identifying their contribution by experiments. However, the short-range vector operators $C^{(9)}_V$ and $\tilde{C}^{(9)}_V$ are associated with a different angular correlation than $m_{\beta\beta}$. On the contrary, the contributions from scalar short-range operators $C^{(9)}_{S2-S5}$ would be hardest to discriminate, as they do not manifest any significant isotope dependence on $R_{im_{\beta\beta}}$ and do not differ in the phase-space observables, either.

In the worst-case scenario, the operators in the group $C^{(6,7)}_{S,V}$, i.e., lepton number violating long-range scalar and vector interactions, are the only operators that result in $R^{\max}_{im_{\beta\beta}} > 2$. In fact, this is the only operator group that is not affected by any unknown LECs. Besides $C^{(6)}_T$ all remaining operators in this setting have expected ratios $R^{\max}_{im_{\beta\beta}} \leq 1.3$, which would require very precise measurements and accurate knowledge of the theoretically calculated half-lives to be able to claim a detection of any of these nonstandard contributions. The contributions from $C^{(6)}_{VL}, C^{(9)}_V$ and $\tilde{C}^{(9)}_V$ could be identified only based on measurements of the angular correlation and the scalar

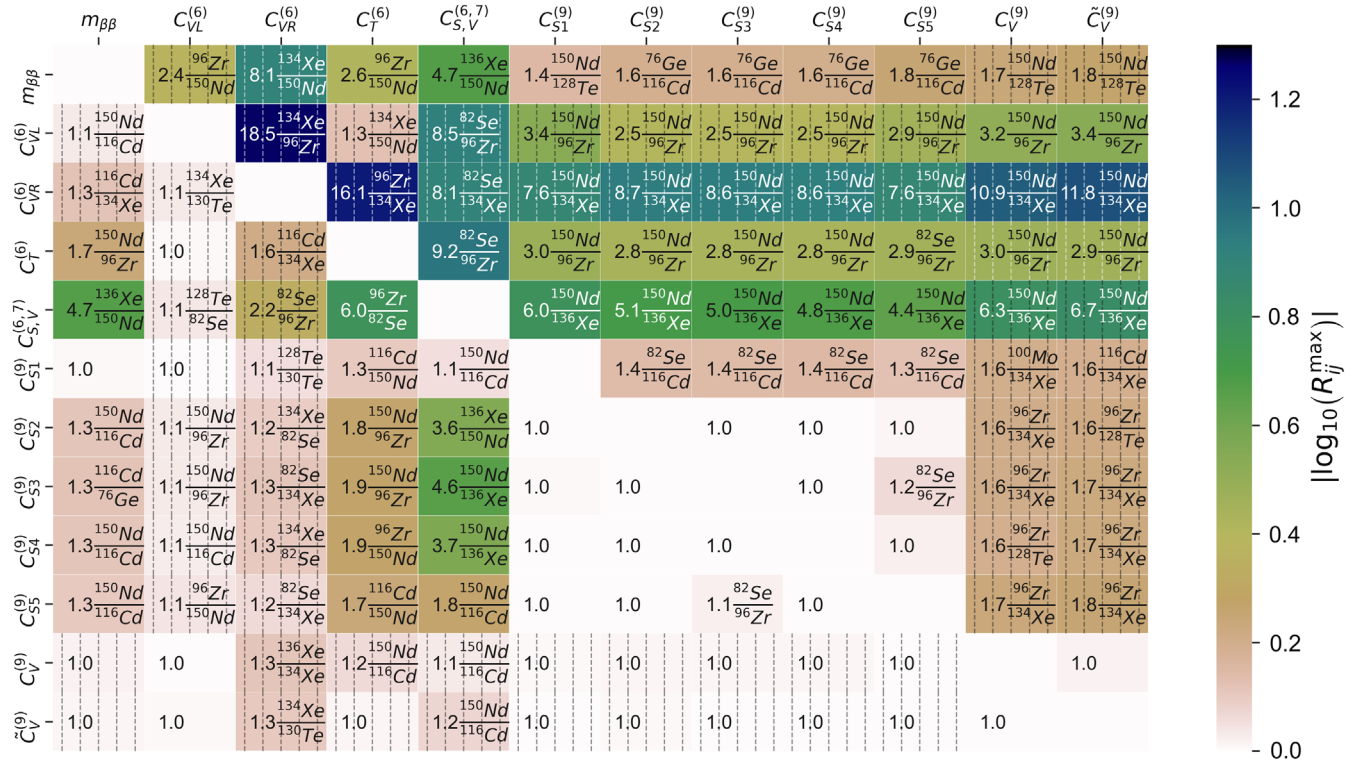

FIG. 8. The maximal ratios $R_{ij}^{\max}$ for all operator combinations i, j. The exact values and the corresponding isotopes are displayed in each tile. Additionally, operator combinations that result in different phase-space observables are marked by dashed-line shading. In the upper right half of the plot we show the ratios considering the central values from the variation of the LECs. In the lower left half we show the worst-case scenario considering the values of ratios R_{ij} that are closest to 1 within the range obtained by the variation of the LECs.

short-range operators, $C_{S1}^{(9)}$, would be completely indistinguishable from the standard mechanism. In Appendix C we show for completeness the same results employing the full set of isotopes, for which there exist numerical values of NMEs computed using IBM2.

To be able to pinpoint the specific nonstandard operator group $\mathcal{O}_j$ contributing to $0\nu\beta\beta$ decay one needs to consider half-life ratios R_{ij} for all different isotopes. Considering the central values, the best candidate to be clearly identified turns out to be the right-handed vector current $C_{VR}^{(6)}$ for which all the ratios $R_{iC_{VR}^{(6)}}^{\max}$ are large, i.e., $\gtrsim 7.6$.

3. The impact of nuclear uncertainties

The uncertainty induced by the nuclear part of the decay rate calculation, i.e., the NMEs and LECs, highly impacts and limits the above approach of distinguishing among different $0\nu\beta\beta$ mechanisms. The approach of comparing theoretically predicted ratios with experimentally measured ratios raises the question of how well these theoretical uncertainties must be under control.

To study the impact of nuclear uncertainties, we can use the general formula for the half-life parametrized in terms of a Wilson coefficient C, the phase-space factor G and an *effective* NME which we label M_{eff},

$$T_{1/2}^{-1} = |C|^2 G |M_{\text{eff}}|^2. \tag{30}$$

Here, M_{eff} is, generally, a weighted sum of combinations of different LECs and NMEs (see Appendix B for the explicit half-life equations of each single operator).

If we consider the theoretical uncertainty of the half-life to be dominated by the uncertainty of M_{eff}, we can determine the necessary theoretical accuracy of the nuclear physics. To estimate this, we assume M_{eff} to be independent of the choice of the isotope, i.e.,

$$\frac{\Delta M_{\text{eff}}}{M_{\text{eff}}}({}^{A}Z) = \frac{\Delta M_{\text{eff}}}{M_{\text{eff}}} = \text{const.} \tag{31}$$

Then the necessary theoretical accuracy can be determined from the simple condition that the expected ratios should be distinguishable from unity within the theoretical uncertainty,

$$\Delta R_{ij} \overset{!}{<} |R_{ij} - 1|. \tag{32}$$

Hence, the necessary theoretical accuracy for M_{eff} reads

$$\frac{\Delta M_{\text{eff}}}{M_{\text{eff}}} \overset{!}{<} \frac{1}{4}\frac{|R_{ij}-1|}{R_{ij}}. \tag{33}$$

Again, taking the central values as a baseline, the theoretical uncertainty on the overall nuclear part (that is from both LECs and NMEs) would need to be brought down to $\frac{\Delta M_{\text{eff}}}{M_{\text{eff}}} \sim 7\%$ to be able to identify all possible nonstandard contributions assuming single operator dominance. The exotic contribution easiest to identify using the half-life ratios would be the right-handed vector current $C_{VR}^{(6)}$ requiring an accuracy of $\frac{\Delta M_{\text{eff}}}{M_{\text{eff}}} \sim 22\%$. We want to emphasize, again, that this way of estimating nuclear uncertainties assumes that our calculations of the central ratios are a reasonable reflection of reality.

In Fig. 9 we show the NME for the standard light-neutrino-exchange mechanism computed employing a variety of different numerical approaches. One can clearly see a significant variation of about a factor of ∼3 with some additional outliers corresponding to the rEDF (CDFT) approach. Given the distinct nature of individual nuclear structure computations the spread of the presented values clearly cannot be interpreted as theoretical uncertainty of the NMEs.

Reaching the estimated required accuracy on both LECs and NMEs seems to be rather challenging considering the current status of the relevant nuclear physics calculations. However, the recent advances in *ab initio* approaches to the computation of $0\nu\beta\beta$ decay NMEs seem to pave the path towards more reliable numerical values and clearer understanding of the theoretical uncertainties involved.

C. Other $0\nu\beta\beta$ modes

Besides the usual $0\nu\beta^-\beta^-$-decay mode one could also make use of searches for neutrinoless modes of other $\beta\beta$ processes. In general there are four of these,

(1) $\beta^-\beta^-$:

$$(A,Z) \to (A,Z+2) + 2e^-(+2\bar{\nu}_e) \tag{34}$$

$$\Delta m \overset{!}{>} 0 \tag{35}$$

(2) $\beta^+\beta^+$:

$$(A,Z) \to (A,Z-2) + 2e^+(+2\nu_e) \tag{36}$$

$$\Delta m \overset{!}{>} 4m_e \tag{37}$$

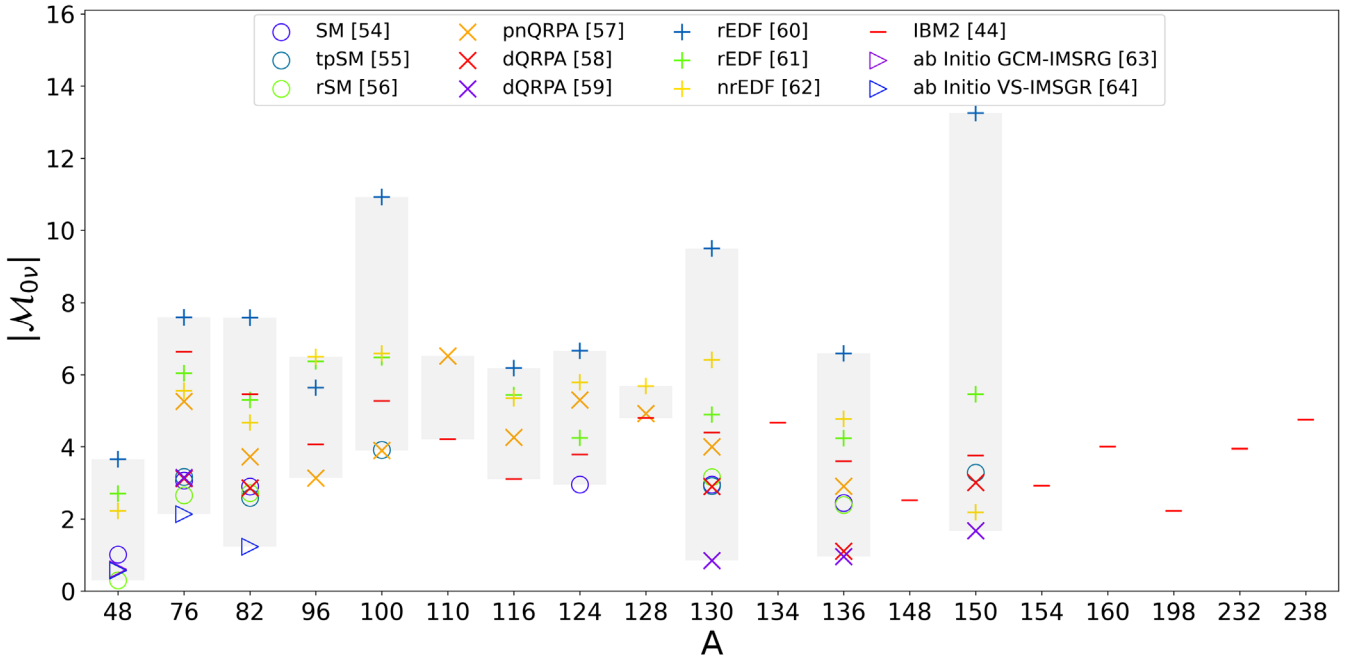

FIG. 9. Comparison of the standard NME $\mathcal{M}_{0\nu} = -\frac{1}{g_A^2}M_F + M_{GT} + M_T$ resulting from different calculation methods. Explicitly, we show NMEs obtained from the interacting shell model (SM) [73] and subsequent variants like the triaxial projected shell model (tpSM) [74] or realistic shell model (rSM) [75], the proton-neutron quasiparticle random phase approximation (pnQRPA) [76], the deformed QRPA (dQRPA) [77,78], the relativistic energy density functional method (rEDF) or covariant density functional theory (CDFT) [79,80], the nonrelativistic energy density functional method (nrEDF) [81], the interacting boson model (IBM2) [12] and recently introduced *ab initio* approaches calculating NMEs from basic principles of χPT [82,83]. The gray bands mark the range of values covered by the different methods.

(3) **ECβ^+**:

$$(A,Z)+e^- \rightarrow (A,Z-2)+e^+(+2\nu_e) \tag{38}$$

$$\Delta m \overset{!}{>} 2m_e \tag{39}$$

(4) **ECEC**:

$$(A,Z)+2e^- \rightarrow (A,Z-2)(+2\nu_e) \tag{40}$$

$$\Delta m \overset{!}{>} 0 \quad 2\nu \text{ mode} \tag{41}$$

$$\Delta m \overset{!}{=} 0 \quad 0\nu \text{ mode}. \tag{42}$$

Here, EC denotes electron capture. In principle, one could study all of these processes, as any of them would help to distinguish different mechanisms using the decay rate ratios considering nuclear uncertainties to be under control. However, all the other $\beta\beta$ processes listed in Table VI are expected to have half-lives significantly longer than the usual $0\nu\beta^-\beta^-$ decay and are therefore unlikely to show up in experiments. Despite that, let us discuss their potential role in a bit more detail.

1. $0\nu\beta^+\beta^+$

This process can be treated in a similar way as the usual $0\nu\beta^-\beta^-$ decay, one only needs to consider a negative nuclear charge $Z \rightarrow -Z$ to calculate the positron wave functions. As such, the expected half-life will also be mainly determined by the PSF which goes with Q^5. Looking at the second column of Table VI we can see that the Q values for naturally occurring isotopes are up to 1 order of magnitude smaller than usual $0\nu\beta^-\beta^-$ Q values. Additionally, the electromagnetic repulsion of the outgoing positrons deforms the wave functions and decreases the decay rate. Thus, we see that $0\nu\beta^+\beta^+$ will be highly suppressed compared to $0\nu\beta^-\beta^-$. Also, given the similarities of the two decays there does not seem to be a natural way of enhancing the $0\nu\beta^+\beta^+$-decay rate with respect to $0\nu\beta^-\beta^-$. The relevant PSFs for the $0\nu\beta^+\beta^+$ decay of naturally occurring isotopes have been calculated in [84] and are about 3–5 orders of magnitude smaller than for $0\nu\beta^-\beta^-$ decay.

2. 0νECβ^+

The PSFs for the neutrinoless mode of ECβ^+ were also calculated with good precision in [84] and are found to be 3–4 orders of magnitude smaller than those corresponding to $0\nu\beta^-\beta^-$ decay. The reason is the same as in the case of $0\nu\beta^+\beta^+$ decay.

3. 0νECEC

As this process has no particles other than the daughter isotope in the final state, mass degeneracy between the mother and daughter isotopes is required in order to satisfy conservation of energy and momentum. However, as the daughter isotope is a nonstable state due to the holes left in the electron shell after the electron capture, the corresponding decay width results in a resonance mechanism [85,86]. Resonances are often found when considering nuclear excitations in the final state isotope. However, the resonant enhancement strongly depends on the degeneracy between the initial and final state and hence small uncertainties in the mass measurements of these nuclei result in considerable uncertainties of the corresponding half-lives [85]. Existing studies tend to show that the resulting half-lives are still considerably longer than for $0\nu\beta^-\beta^-$ [86]. Therefore, we do not consider this process in this work. However, it is fair to note that a close resonance might lead to half-lives comparable or even shorter than for $0\nu\beta^-\beta^-$ decay. Recently, it was shown that further significant enhancement of the 0νECEC decay rate can be generated by a nonresonance shake mechanism [87]. In this case, the double electron capture is accompanied by emission of an electron from the shell of the final state isotope, which can carry away energy, thus making the whole process less dependent on the resonant behavior. A dedicated review of the 0νECEC decay can be found in [88].

4. Bound-state $0\nu\beta\beta$

Bound state $0\nu\beta\beta$ decay refers to a decay in which one or both of the two outgoing electrons end up in a bound energy level of the daughter isotope. It is usually referred to as $0\nu\beta$EP and 0νEPEP for the one and two bound final state electrons, respectively, with EP denoting the electron production or electron placement. Being a reverse process of 0νECEC, also 0νEPEP requires mass degeneracy of the initial and final nuclei and the decay rate is described by a resonancelike mechanism. The explicit calculations show that the corresponding half-lives are even longer than those of double electron capture [85]. The reason is that there are no electron holes in the shell and only the (small) decay width of the nuclear excitation enters into the resonance.

The single bound state double-β-decay $0\nu\beta$EP was investigated in [89] and found to have PSFs 6–7 orders of magnitude smaller than those of $0\nu\beta^-\beta^-$ decay. The decay rates can be significantly enhanced when considering fully ionized nuclei. In that case, the $0\nu\beta$EP decay rate can for certain isotopes even exceed the one of $0\nu\beta^-\beta^-$ decay [89]. Although this is an interesting idea, a full ionization of large number of isotopes represents an experimental challenge. Therefore, despite the enhanced decay rate, the number of available ions would be too small to reach the relevant experimental sensitivity.

5. Decay to excited final state nuclei

Instead of utilizing different isotopes to determine the decay rate ratios one could also compare the ground state decay with the decay into an excited state final nucleus $(0^+, 2^+)$ using the same initial state isotope [90,91]. The potential benefit would be the possibility of studying this interplay within a single experiment. However, the excited state decays can be again expected to be highly suppressed due to the smaller phase space resulting from the smaller Q value. Additionally, previous studies tend to show that the NMEs for the decay into the excited final state are either of a similar size or smaller than those for the ground state decay [91–93], thus the half-lives would be rather further suppressed than enhanced by the nuclear part of the amplitude either.

6. Artificial isotopes

Although there are 69 naturally occurring double-β-decaying isotopes, we found about ~2700 possible $0\nu\beta\beta$ candidate isotopes when considering the full NIST list of elements [94]. Some of them have considerably larger Q values of up to 50 MeV.[2] While such a large Q value of ~50 MeV would result in a significant enhancement of the decay rate by ~8 orders of magnitude, there are several fairly obvious experimental problems. Primarily, it is the artificial production of these isotopes which would strongly limit the scale of the experiment. Again ton, kilogram and even gram scales would usually not be possible. Additionally, many artificial isotopes, especially those with large Q values, come with additional decay modes that strongly dominate and often lead to extremely short half-lives such that storing them to study $0\nu\beta\beta$ decay would be impossible.

To sum up the above paragraphs, despite the fact that a variety of $\beta\beta$ processes exist, $0\nu\beta^-\beta^-$ decay is largely the most relevant candidate to study, indeed. Therefore, other possible $0\nu\beta\beta$ modes would only become relevant in exotic scenarios leading either to their significant enhancements, or to strong suppression of $0\nu\beta^-\beta^-$ decay. Given the similarity of all the $\beta\beta$ processes, such models would, however, seem to be rather unnatural from a particle physics point of view.

IV. DISTINGUISHING SPECIFIC MODELS

Following the discussion of possible discrimination among different LEFT operators, let us now have a brief look at complete models. As one would expect, lepton number violating BSM models will typically excite several LEFT operators at a time. While it would be challenging to identify a specific BSM model, as no finite set of BSM models exists and many different scenarios would result in the same low-energy physics, we do expect that, given fixed model parameters, one can at least check whether a model is consistent with the observed data and reject it if it is not. In the following paragraphs, we adopt and briefly discuss three different BSM scenarios that would lead to $0\nu\beta\beta$ decay. Each of the models will be compared with the standard mass mechanism predictions.

A. Minimal left-right symmetric model

The Standard Model is a chiral theory. That is, parity is explicitly broken due to the gauged $SU(2)_L$ symmetry and the missing right-handed neutrino. This particular choice of symmetries and particle content, additionally, results in vanishing neutrino masses. A simple approach to resolve these phenomena is to extend the Standard Model's gauge group to a left-right symmetric model $SU(3)_C \times SU(2)_L \times SU(2)_R \times U(1)_{B-L}$ [95–97] which is spontaneously broken to the Standard Model group $SU(3)_C \times SU(2)_L \times U(1)_Y$. A comprehensive review of the minimal left-right symmetric Standard Model (mLRSM) is given in, e.g., [98].

Extending the Standard Model to the left-right symmetric theory requires the existence of additional scalars and fermions. The conventional minimal setting includes two scalar triplets $\Delta_L \in (1,3,1,2)$ and $\Delta_R \in (1,1,3,2)$ as well as a scalar bidoublet $\Phi \in (1,2,2^*,0)$ incorporating the SM Higgs doublet and the right-handed neutrinos ν_R. The fermions are grouped into left- and right-handed doublets,

$$L_L = \begin{pmatrix} \nu_L \\ e_L \end{pmatrix} \in (1,2,1,-1), \quad Q_L = \begin{pmatrix} u_L \\ d_L \end{pmatrix} \in (3,2,1,1/3), \tag{43}$$

$$L_R = \begin{pmatrix} \nu_R \\ e_R \end{pmatrix} \in (1,1,2,-1), \quad Q_R = \begin{pmatrix} u_R \\ d_R \end{pmatrix} \in (3,1,2,1/3), \tag{44}$$

which under $U \in SU(2)_{L,R}$ transform as

$$\Psi_{L,R} \to U_{L,R}\Psi_{L,R} \tag{45}$$

while the scalar fields transform as

$$\Phi \to U_L \Phi U_R^\dagger, \qquad \Delta_L \to U_L \Delta_L U_L^\dagger, \qquad \Delta_R \to U_R \Delta_R U_R^\dagger. \tag{46}$$

There are two discrete symmetries that one can impose onto a LR symmetric theory which can relate left- and right-handed fermions. These are parity P and charge conjugation C [99]. Thus, one can define two different discrete symmetry transformations:

$$P\colon \Psi_L \Leftrightarrow \Psi_R, \qquad \Phi \Leftrightarrow \Phi^\dagger, \qquad \Delta_{L,R} \Leftrightarrow \Delta_{R,L} \tag{47}$$

[2]Considering only isotopes without a single-β-decay mode already significantly reduces this number down to 86. None of these has, however, a significantly enhanced Q value.

$$C\colon\ \Psi_L \Leftrightarrow (\Psi_R)^c, \qquad \Phi \Leftrightarrow \Phi^T, \qquad \Delta_{L,R} \Leftrightarrow \Delta^*_{R,L}. \quad (48)$$

Requiring either P or C invariance results in different constraints on the scalar potential as well as the Yukawa coupling matrices [99].[3]

The lepton number violation at low energy stems from the leptonic Yukawa interactions given by

$$\mathcal{L}_y = -\sum_{ij}\{(Y^{l\dagger})_{ij}\overline{L_{Li}}\Phi L_{R,j} + (\tilde{Y}^{l\dagger})_{ij}\overline{L_{Li}}\tilde{\Phi}L_{R,j} + Y^L_{ij}L^T_{L,i}Ci\tau_2\Delta_L L_{L,j} + (Y^{R\dagger})_{ij}L^T_{R,i}Ci\tau_2\Delta_R L_{R,j}\} + \text{H.c.} \quad (49)$$

After the neutral components of the scalars have acquired their VEVs,

$$\langle\Phi\rangle = \frac{1}{\sqrt{2}}\begin{pmatrix}\kappa & 0\\ 0 & \kappa' e^{i\alpha}\end{pmatrix},$$
$$\langle\Delta_L\rangle = \frac{1}{\sqrt{2}}\begin{pmatrix}0 & 0\\ v_L e^{i\theta_L} & 0\end{pmatrix},$$
$$\langle\Delta_R\rangle = \frac{1}{\sqrt{2}}\begin{pmatrix}0 & 0\\ v_R & 0\end{pmatrix}, \quad (50)$$

one can infer the neutrino mass matrices from (49)

$$M^\nu_{D,ij} = \frac{1}{\sqrt{2}}[Y^l_{ij}\kappa + \tilde{Y}^l_{ij}\kappa' \exp -i\alpha],$$
$$M^\nu_{L,ij} = \sqrt{2}Y^L_{ij}v_L \exp i\theta_L,$$
$$M^\nu_{R,ij} = \sqrt{2}Y^R_{ij}v_R. \quad (51)$$

There are several diagrams in the mLRSM setting which can contribute to the $0\nu\beta\beta$ decay at tree level, see Fig. 10. Detailed discussions of $0\nu\beta\beta$ decay within the mLRSM scenario can be found, e.g., in [8,18,23].

The matching of the C-symmetric mLRSM onto SMEFT and, subsequently, onto the relevant LEFT operators has been discussed in [10]. Here, we will summarize their findings and study the distinguishability from the usual mass mechanism.

Integrating out the heavy fields with masses proportional to v_R and matching the theory onto SMEFT results in the lepton number violating operators,

$$\mathcal{L}_{\Delta L} = C^{(5)}((L^T Ci\tau_2\Phi_{\rm SM})(\tilde{\Phi}^\dagger_{\rm SM}L)) + (L^T\gamma^\mu e_R)i\tau_2\Phi_{\rm SM}(C^{(7)}_{Leu\bar{d}\Phi}\overline{d_R}\gamma_\mu u_R + C^{(7)}_{L\Phi De}\Phi^T_{\rm SM}i\tau_2(D_\mu\Phi_{\rm SM})) + \overline{e_R}e^c_R(C^{(9)}_{eeud}\overline{u_R}\gamma^\mu d_R\overline{u_R}\gamma_\mu d_R + C^{(9)}_{ee\Phi ud}\overline{u_R}\gamma^\mu d_R([iD_\mu\Phi_{\rm SM}]^\dagger\tilde{\Phi}_{\rm SM}) + C^{(9)}_{ee\Phi D}([iD_\mu\Phi_{\rm SM}]^\dagger\tilde{\Phi}_{\rm SM})^2), \quad (52)$$

where $\Phi_{\rm SM}$ is the Standard Model Higgs doublet. The matching scale corresponds to $\sim m_{W_R}$ and the Wilson coefficients at SMEFT level are given by

$$C^{(5)} = \frac{1}{v^2}(M^{\nu\,T}_D M^{\nu\,-1}_R M^\nu_D - M^\nu_L),$$
$$C^{(7)}_{Leu\bar{d}\Phi} = \frac{\sqrt{2}}{v}\frac{1}{v_R^2}(V^{ud}_R)^*(M^{\nu T}_D M^{\nu\,-1}_R)_{ee},$$
$$C^{(7)}_{L\Phi De} = \frac{2i\xi\exp i\alpha}{(1+\xi^2)V^{ud*}_R}C^{(7)}_{Leu\bar{d}\Phi},$$
$$C^{(9)}_{eeud} = -\frac{1}{2v_R^4}V^{ud2}_R\left[(M^{\nu\,\dagger}_R)^{-1} + \frac{2}{m^2_{\Delta_R}}M^\nu_R\right],$$
$$C^{(9)}_{ee\Phi ud} = -4\frac{\xi\exp -i\alpha}{(1+\xi^2)V^{ud}_R}C^{(9)}_{eeud},$$
$$C^{(9)}_{ee\Phi D} = 4\frac{\xi^2\exp -2i\alpha}{(1+\xi^2)^2V^{ud2}_R}C^{(9)}_{eeud}, \quad (53)$$

where v is the Standard Model Higgs doublets VEV,

$$v^2 = \kappa^2 + \kappa'^2. \quad (54)$$

Here, $C^{(5)}$ corresponds to the usual seesaw formula. From the matching scale $\sim m_{W_R}$ the above coefficients have to be evolved down to $m_W \sim 80$ GeV, at which one can match onto the relevant LEFT operators by integrating out the remaining heavy particles with masses above m_W. By doing so, one obtains

$$m_{\beta\beta} = -v^2C^{(5)}_{ee}$$
$$C^{(6)}_{VL} = -iV^{ud}_L\frac{v^3}{\sqrt{2}}C^{(7)\,*}_{L\Phi De},$$
$$C^{(6)}_{VR} = \frac{v^3}{\sqrt{2}}C^{(7)\,*}_{Leu\bar{d}\Phi},$$
$$C^{(9)}_{1R}(m_W) = v^5V^{ud2}_L C^{(9)}_{ee\Phi D}(m_W),$$
$$C^{(9)\prime}_{1R}(m_W) = v^5C^{(9)}_{eeud}(m_W),$$
$$C^{(9)}_{4R}(m_W) = -v^5V^{ud}_L C^{(9)}_{ee\Phi ud}(m_W). \quad (55)$$

[3]Note that a combination of both does not fit observational constraints [99].

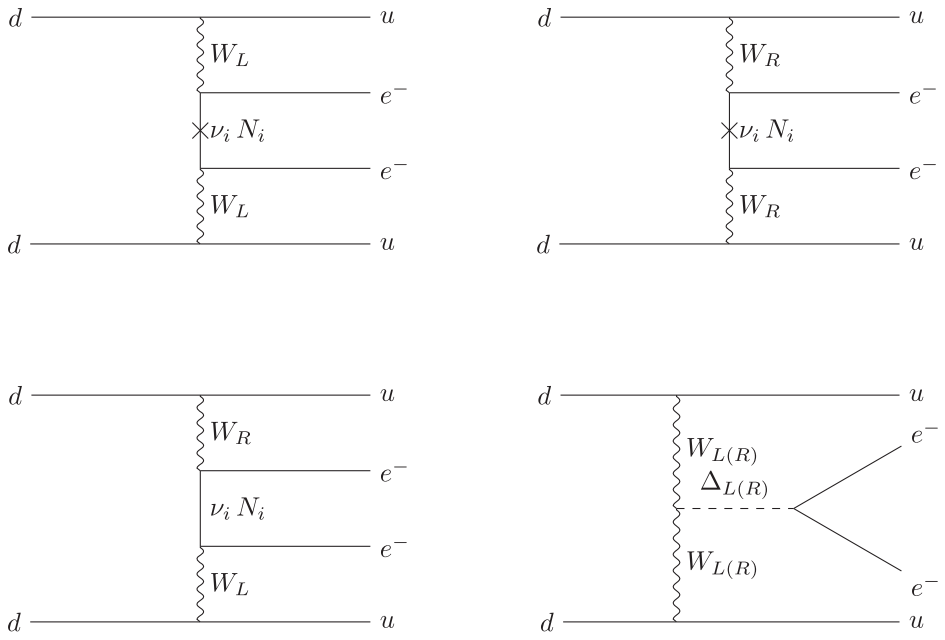

FIG. 10. Feynman diagrams arising in the mLRSM that contribute to $0\nu\beta\beta$. Here, ν_i and N_i represent the light and heavy neutrino mass eigenstates. It should be noted that, due to mixing of both left- and right-handed neutrinos and gauge bosons, each diagram (except the triplet-exchange diagram) comes with all possible combinations of the outgoing particle's chiralities. However, some diagrams are highly suppressed compared to others.

Evolving the above coefficients down to the χPT scale of $\sim$2 GeV also generates a nonzero $C_{5R}^{(9)}$ coefficient since the renormalization group equations of $C_{4,5}^{(9)}$ mix.

The relevant Wilson coefficients are fixed by several physical parameters: the values of the triplet VEVs $v_{L,R}$, the mass of the heavy right-handed triplet $m_{\Delta R}$ as well as the masses of the three heavy neutrinos $(m_{\nu_{R1}}, m_{\nu_{R2}}, m_{\nu_{R3}})$ and the lightest neutrino mass $m_{\nu_{\rm min}}$, the complex phases of the VEVs α and θ_L and finally the left-right mixing parameter ξ. Here, we fix $\xi = \frac{m_b}{m_t}$. The lightest neutrino mass together with the squared mass differences Δm_{ij}^2 that are known from oscillation data fix the remaining light neutrino masses for a given mass hierarchy. Taking

$$|\nu_{\alpha L,R}\rangle = \sum_i U_{\alpha i}^* |\nu_{iL,R}\rangle \tag{56}$$

we obtain

$$\begin{aligned} M_\nu &= v^2 C^{(5)} = U_{\rm PMNS} m_\nu U_{\rm PMNS}^T \\ m_\nu &= {\rm diag}(m_{\nu_1}, m_{\nu_2}, m_{\nu_3}), \end{aligned} \tag{57}$$

and

$$\begin{aligned} M_R^\nu &= U_R m_{\nu R} U_R^T \\ m_{\nu R} &= {\rm diag}(m_{\nu_{R1}}, m_{\nu_{R2}}, m_{\nu_{R3}}). \end{aligned} \tag{58}$$

Additionally, the mixing matrix U for the heavy neutrinos must be fixed. Here, we take $U_R = U_{\rm PMNS}$ for simplicity. In the C-symmetric case, one has

$$M_L^\nu = \frac{v_L \exp i\theta_L}{v_R} M_\nu^R \tag{59}$$

and the Dirac mass matrix can be derived as [100]

$$M_D^\nu = U_{\rm PMNS} m_{\nu_R} \sqrt{\frac{v_L \exp i\theta_L}{v_R} \mathbb{1}_{(3\times3)} - m_{\nu R}^{-1} m_\nu} U_{\rm PMNS}^T. \tag{60}$$

Assuming $V_L^{ud} = V_R^{ud}$ and

$$\begin{aligned} &m_{\nu_{R1}} = 10\ {\rm TeV}, \quad m_{\nu_{R2}} = 12\ {\rm TeV}, \quad m_{\nu_{R3}} = 13\ {\rm TeV} \\ &m_{\Delta_R} = 4\ {\rm TeV}, \quad v_L = 0.1\ {\rm eV} \quad v_R = 10\ {\rm TeV} \end{aligned} \tag{61}$$

as in [10], we can derive the LEFT Wilson coefficients in dependence on the minimal light neutrino mass $m_{\rm min}$, the Majorana phases entering $U_{\rm PMNS}$ and the VEV phases θ_L and α.

The resulting phase-space observables in this parameter setting of the mLRSM are hardly any different from the standard mechanism. This is because of the specific choice of parameters studied here which results in the scalar short-range contributions dominating over the long-range

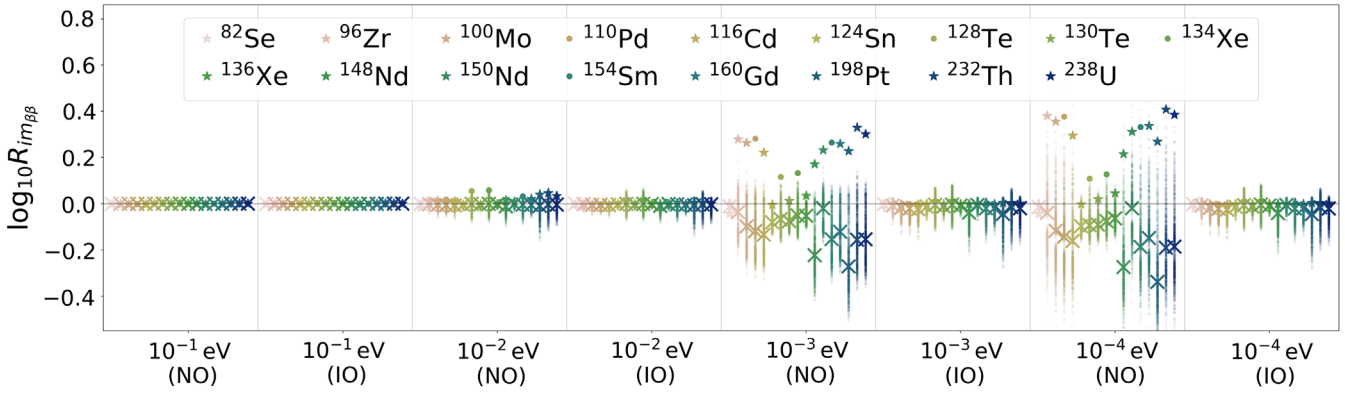

FIG. 11. Half-life ratios resulting from different mLRSM settings (different neutrino mass hierarchy and different minimal neutrino mass) when taking ^{76}Ge as the reference isotope. The ratios are compared to the standard mass mechanism. We vary both the unknown LECs as well as the unknown phases of the mLRSM model.

contributions. Hence, the phase space is almost indistinguishable from the standard mechanism.

The resulting half-life ratios normalized to the standard mass mechanism are depicted in Fig. 11. Here, in additional to varying the unknown LECs we also marginalized over the unknown phases. We can see that assuming inverted mass ordering there are only minor variations from the standard mechanism. In the case of normal ordering, the nonstandard contributions alter the ratios notably only for small $m_{\min} \leq 10^{-3}$ eV. In this region, as shown before in Fig. 5, the central values of the variation differ significantly from the benchmark scenario. A similar behavior is manifested in Fig. 12 displaying the half-life in dependence on the minimal neutrino mass $m_{\min}$ for both orderings and in comparison with the standard mechanism on its own. One can see that in the case of inverted ordering the half-life is almost unaltered from the standard mechanism while for normal ordering the nonstandard contributions start to play a substantial role below $\sim 10^{-2}$ eV decreasing the expected half-life by about 1 order of magnitude compared to the standard scenario. In the same range of $m_{\min}$ the uncertainties induced by the unknown LECs start to significantly influence the predicted half-life. On the other hand, the central values of the decay rate ratios alter for $m_{\min} \lesssim 10^{-3}$ eV at most by a factor of $R^{\max}_{im_{\beta\beta}} \sim 2.2$ with ^{76}Ge as the reference isotope. The reason for this behavior can be traced back to the dominance of the short-range contributions which (see Sec. III) result in relatively small $R_{im_{\beta\beta}}$ despite the appearance of $C^{(6)}_{VR}$. This ratio would translate to a necessary accuracy on the nuclear part of the amplitude of $\frac{\Delta M_{\text{eff}}}{M_{\text{eff}}} \lesssim 14\%$.

B. Gluino and neutralino exchange in $\not{R}_p$-SUSY

Supersymmetric theories contain supermultiplets of fermions and bosons which, under supersymmetry, transform into each other. The most simple constructions are chiral supermultiplets

$$(\Psi_{L,R}, \Phi^{\Psi}_{L,R}) \tag{62}$$

which relate two component chiral spinors $(\Psi_{L,R})$ and a corresponding complex scalar $\Phi_{L,R}$. To construct a supersymmetric version of the Standard Model, one also needs to consider gauge supermultiplets

$$(A^a_\mu, \Psi^a) \tag{63}$$

which relate the Standard Model's gauge bosons A^a_μ to their superpartner fermions Ψ^a. One should note that since gauge

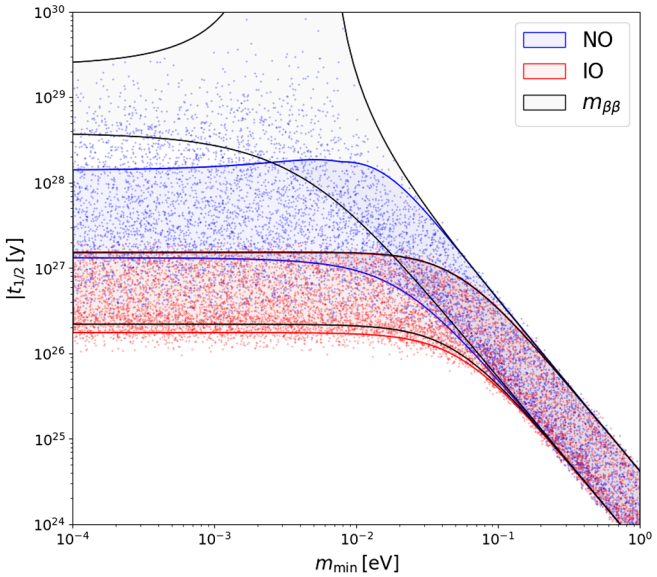

FIG. 12. Here we present the half-life of ^{76}Ge in the mLRSM model in dependency on the minimal neutrino mass $m_{\min}$ for both normal (NO) and inverted ordering (IO). The blue and red areas represent the scenario marginalized over the unknown phases with the LECs fixed to their order of magnitude estimate while the scattered points show the additional variation of the relevant LECs. The area inside the black borders represents the usual mass mechanism without any additional contributions.

bosons have 2 degrees of freedom (d.o.f.) and since this kind of transformation obviously cannot change the number of d.o.f., their superpartners Ψ^a also have 2 degrees of freedom. Therefore, they are Majorana fermions. As particles within a supermultiplet must share the same mass, quantum numbers (except spin), interactions and couplings, supersymmetry (SUSY) must be broken at low energies to reproduce the experimentally confirmed SM predictions. Typically, after SUSY breaking there remains a discrete symmetry called R parity (R_p) which can be assigned to every field, such that we have $R_p = +1$ for Standard Model fields and $R_p = -1$ for the superpartner fields. One can define R parity as [101]

$$R_p = (-1)^{2s+3(B-L)}, \tag{64}$$

where s is the spin and B and L are the corresponding baryon and lepton numbers of the field, respectively. If R_p is a conserved quantity, it follows that the lightest superpartner cannot decay such that it becomes a candidate for explaining the origin of dark matter.

However, R_p conservation also comes with the conservation of both baryon and lepton number [101]. Thus, supersymmetric models aiming to explain the baryon asymmetry of the Universe via explicit violation of either lepton or baryon number need to break R_p. This induces new lepton number violating terms [102],

$$\mathcal{L}^{\Delta L=1}_{\not R_p} = -\lambda'_{111}\left[(\overline{u_L}, \overline{d_R})\begin{pmatrix} e^c_L \\ -\nu^c_L \end{pmatrix}\tilde{d}_R + (\overline{e_L}, \overline{\nu_L})d_R\begin{pmatrix} \tilde{u}^*_L \\ -\tilde{d}^*_L \end{pmatrix} + (\overline{u_L}, \overline{d_L})d_R\begin{pmatrix} \tilde{e}^*_L \\ -\tilde{\nu}^*_L \end{pmatrix}\right] + \text{H.c.}, \tag{65}$$

which can contribute to $0\nu\beta\beta$ decay. Contributions to $0\nu\beta\beta$ decay from $\not R_p$-SUSY have been studied first in Refs. [102,103], the corresponding Feynman diagrams are shown in Fig. 13. The relevant gluino ($\tilde{g}$) and neutralino (χ)-fermion interactions are given by [102,104,105]

$$\mathcal{L}_{\tilde{g}} = -\sqrt{2}g_3\sum_a \frac{\lambda^{(a)}_{\alpha\beta}}{2}(\overline{q_L}^\alpha \tilde{g}\tilde{q}^\beta_L - \overline{q_R}^\alpha \tilde{g}\tilde{q}^\beta_R) + \text{H.c.} \tag{66}$$

and

$$\mathcal{L}_\chi = \sqrt{2}g_2\sum_{i=1}^{4}(\epsilon_{Li}(\Psi)\overline{\Psi_L}\chi_i\tilde{\Psi}_L + \epsilon_{Ri}(\Psi)\overline{\Psi_R}\chi_i\tilde{\Psi}_R +) + \text{H.c.} \tag{67}$$

One can obtain the low-energy effective Lagrangian by integrating out the heavy superfields as well as the Standard Model particles with masses $\gtrsim m_W$. In doing so, one finds the different low-energy effective dimension-9 $\Delta L = 2$ operators that contribute to $0\nu\beta\beta$ decay [103]:

$$\begin{aligned}\mathcal{L}_{\not R_p} =& \frac{G_F^2}{2m_N}[\bar{e}(1+\gamma_5)e^c] \\ &\times\Bigg[(\eta_{\tilde{g}}+\eta_\chi)\Bigg([\bar{u}(1+\gamma^5)d][\bar{u}(1+\gamma^5)d] \\ &-\frac{1}{4}[\bar{u}\sigma^{\mu\nu}(1+\gamma^5)d][\bar{u}\sigma_{\mu\nu}(1+\gamma^5)d]\Bigg) \\ &+(\eta_{\chi\tilde{e}}+\eta_{\tilde{g}\prime}-\eta_{\chi\tilde{f}})[\bar{u}(1+\gamma^5)d][\bar{u}(1+\gamma^5)d]\Bigg].\end{aligned} \tag{68}$$

These can be matched onto the LEFT basis as

$$\begin{aligned}C^{(9)\prime}_{2R} &= \frac{2v}{m_N}[2\eta_{\tilde{g}} + 2\eta_\chi + \eta_{\chi\tilde{e}} + \eta_g{}' - \eta_{\chi\tilde{f}}] \\ C^{(9)\prime}_{3R} &= \frac{4v}{m_N}[\eta_{\tilde{g}} + \eta_\chi].\end{aligned} \tag{69}$$

The coupling constants are given in terms of gluino, neutralino and squark masses as [102]

$$\begin{aligned}\eta_{\tilde{g}} &= \alpha_s\lambda^2\frac{m_N}{m_{\tilde{g}}}\left[1+\left(\frac{m_{\tilde{d}_R}}{m_{\tilde{u}_L}}\right)^4\right] \\ \eta_{\tilde{g}}{}' &= 2\alpha_s\lambda^2\frac{m_N}{m_{\tilde{g}}}\left(\frac{m_{\tilde{d}_R}}{m_{\tilde{u}_L}}\right)^2 \\ \eta_\chi &= \frac{3\alpha_2}{4}\lambda^2\sum_{i=1}^{4}\frac{m_N}{m_{\chi_i}}\left[\epsilon^2_{Ri}(d)+\epsilon^2_{Li}(u)\left(\frac{m_{\tilde{d}_R}}{m_{\tilde{u}_L}}\right)^4\right] \\ \eta_{\chi\tilde{e}} &= 9\alpha_2\lambda^2\left(\frac{m_{\tilde{d}_R}}{m_{\tilde{e}_L}}\right)^4\sum_{i=1}^{4}\epsilon^2_{Li}(e)\frac{m_N}{m_{\chi_i}} \\ \eta_{\chi\tilde{f}} &= \frac{3\alpha_2}{2}\lambda^2\left(\frac{m_{\tilde{d}_R}}{m_{\tilde{e}_L}}\right)^2\sum_{i=1}^{4}\frac{m_N}{m_{\chi_i}}\Bigg[\epsilon_{Ri}(d)\epsilon_{Li}(e) \\ &\quad+\epsilon_{Ri}(u)\epsilon_{Li}(d)\left(\frac{m_{\tilde{e}_L}}{m_{\tilde{u}_L}}\right)^2 \\ &\quad+\epsilon_{Ri}(u)\epsilon_{Li}(e)\left(\frac{m_{\tilde{d}_R}}{m_{\tilde{u}_L}}\right)^2\Bigg]\end{aligned} \tag{70}$$

with

$$\lambda = \frac{\sqrt{2\pi}}{3}\frac{\lambda'_{111}}{G_F m^2_{\tilde{d}_R}}. \tag{71}$$

Both gluino- and neutralino-exchange diagrams contribute to the same low-energy operators. As pointed out in the previous section, distinguishing between the different contributions triggered by $C^{(9)\prime}_{2R}$ and $C^{(9)\prime}_{3R}$ is practically impossible due to the unknown LECs. Given that both operators contribute only to G_{01}, the phase-space

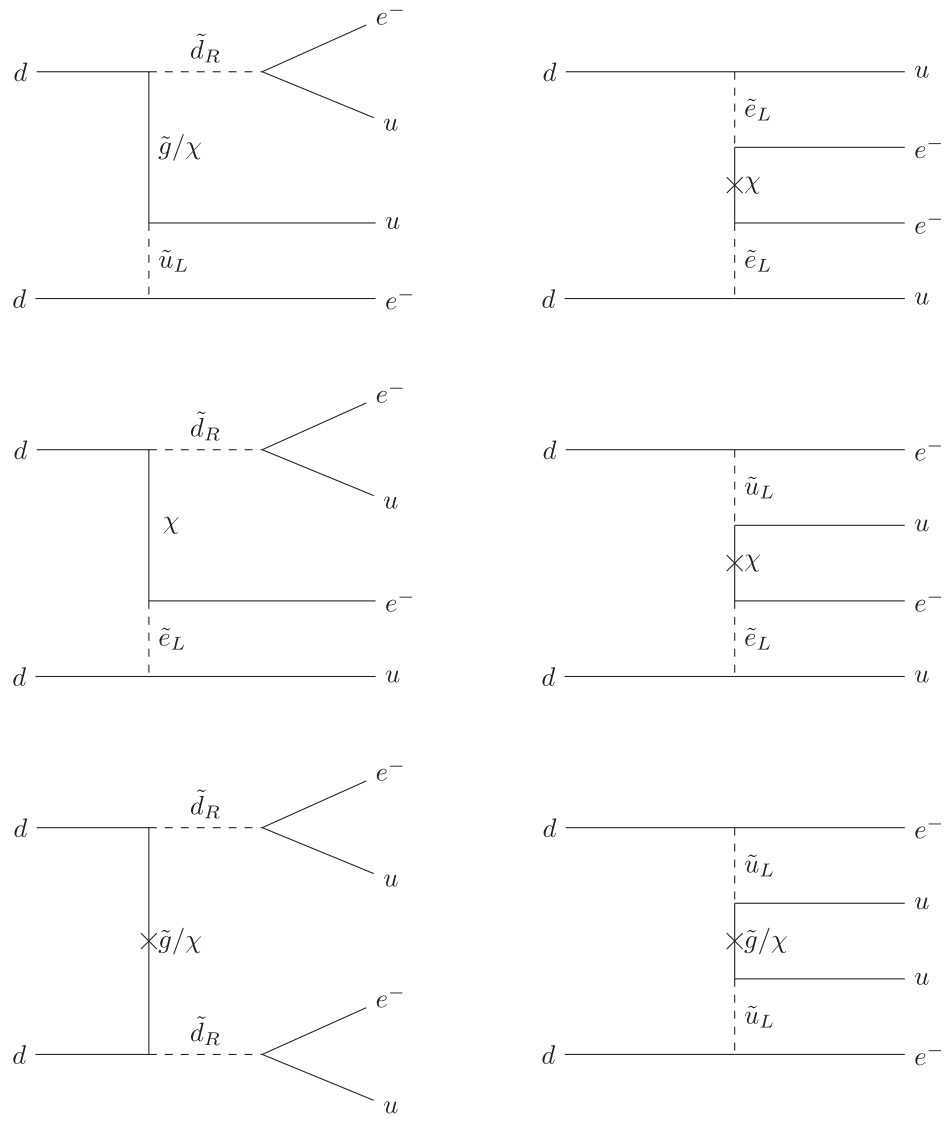

FIG. 13. Feynman diagrams of gluino and neutralino exchange contributing to $0\nu\beta\beta$ within the $\not{R}_p$-minimal supersymmetric Standard Model [102].

observables do not provide any additional information either. For completeness, we present the ratios normalized to the mass mechanism in Fig. 14. Clearly, the $\not{R}_p$-SUSY model we consider here follows the same pattern as the scalar short-range operators $C_{2R}^{(9)}$ and $C_{2R}^{(9)\prime}$ already discussed in Sec. III. In Fig. 15 we show the expected half-life assuming the simultaneous existence of the standard mass mechanism and the $\not{R}_p$-SUSY induced mechanisms. Here, we assume the masses of the non-neutralino superpartners to be given by the current experimental limits, i.e., $m_{\tilde{e}_L} = 410$ GeV, $m_{\tilde{q}_{L,R}} = 1600$ GeV with $q \in [u, d]$ and $m_{\tilde{g}} = 2260$ GeV [106]. We fix the neutralino masses by requiring that the applied EFT framework holds, which necessitates $m_{\chi_i} \geq \Lambda_\chi \simeq 2$ GeV. For simplicity we take $m_{\chi_1} = 2$ GeV and $m_{\chi_i} \to \infty$ for $i \neq 1$. Lighter neutralino masses in connection to $0\nu\beta\beta$ have also recently been studied [107]. We set the coupling constant to $\lambda'_{111} = 2 \times 10^{-4}$. Similarly to the mLRSM discussed above, the additional nonstandard contributions hardly affect the inverted ordering setting. However, in the normal ordering case the nonstandard contributions from the $\not{R}_p$-SUSY model start to significantly influence the expected half-lives decreasing them, again, by about 1 order of magnitude. While one would naively assume that this should result in significantly enhanced ratios, it is important to bear in mind that any enhancement in the decay rates which is independent of the isotope of interest will drop out when considering the decay rate ratios.

C. Leptoquark models

Leptoquarks (LQs) are hypothetical bosons $(3, X, Y)$ with nonzero color charge which couple to both quarks and

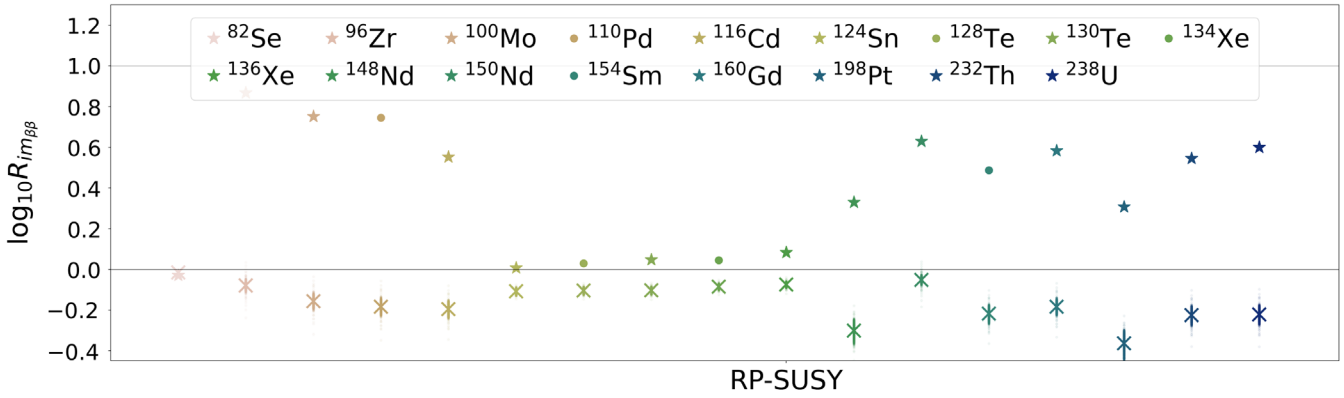

FIG. 14. Half-life ratios resulting from the $\not{R}_p$-SUSY contributions to $0\nu\beta\beta$ normalized to the standard mass mechanism.

leptons. They appear in numerous Standard Model extensions such as technicolor and composite models [108,109] or grand unifications [110,111] and can be used to generate neutrino masses at the one-loop level [112]. For a comprehensive review on leptoquarks see, e.g., [113].

Ignoring leptoquarks which do not directly couple to the Standard Model's particle content (i.e., without right-handed neutrinos), one can add up to ten different leptoquarks obeying the Standard Model symmetries [114]. These are summarized in Table V. By looking at the relevant Feynman diagrams in Fig. 16 we can see that the contributions to $0\nu\beta\beta$ decay arise from leptoquarks with $Q^{(1)} = \pm 1/3$ [Fig. 16 (left)] and $Q^{(2)} = \pm 2/3$ [Fig. 16 (right)]. The full set of renormalizable LQ-fermion interactions is given by [114]

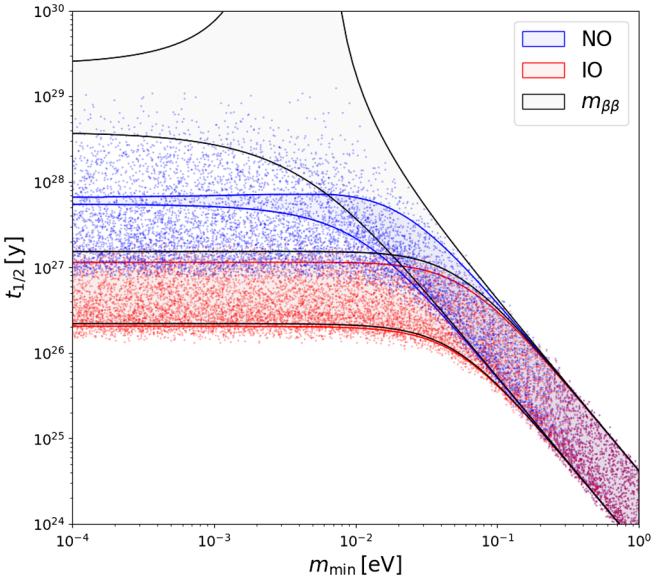

FIG. 15. Half-lives in ^{76}Ge for the standard mass mechanism accompanied by the exchange of heavy neutralinos and gluinos in the $\not{R}_p$-SUSY with $\lambda'_{111} = 2 \times 10^{-4}$, $m_{\tilde{e}_L} = 410$ GeV, $m_{\tilde{q}_{L,R}} = 1600$ GeV, $m_{\tilde{g}} = 2260$ GeV, $m_{\chi_1} = \Lambda_\chi = 2$ GeV and $m_{\chi_i} \to \infty$ for $i \neq 1$.

$$\begin{aligned}\mathcal{L}_{S,f} = {} & (\lambda^R_{S_0})_{ij} S_0^{R\dagger}[\overline{u^c}_i P_R e_j] + (\lambda^R_{\tilde{S}_0})_{ij} \tilde{S}_0^{\dagger}[\overline{d^c}_i P_R e_j] \\ & + (\lambda^R_{S_{1/2}})_{ij} S_{1/2}^{R\dagger}[\overline{u}_i P_L L_j] + (\lambda^R_{\tilde{S}_{1/2}})_{ij} \tilde{S}_{1/2}^{\dagger}[\bar{d}_i P_L L_j] \\ & + (\lambda^L_{S_0})_{ij} S_0^{L\dagger}[\overline{Q^c}_i P_L i\tau_2 L_j] + (\lambda^L_{S_{1/2}})_{ij} S_{1/2}^{L\dagger}[\overline{Q^c}_i P_R i\tau_2 e_j] \\ & + (\lambda^L_{S_1})_{ij} [\overline{Q^c}_i P_L i\tau_2 S_1^{\dagger} L_j] + \text{H.c.} \end{aligned} \tag{72}$$

and

$$\begin{aligned}\mathcal{L}_{V,f} = {} & (\lambda^R_{V_0})_{ij} V_{0\mu}^{R\dagger}[\overline{d}_i \gamma^\mu P_R e_j] + (\lambda^R_{\tilde{V}_0})_{ij} \tilde{V}_{0\mu}^{R\dagger}[\bar{u}_i \gamma^\mu P_R e_j] \\ & + (\lambda^R_{V_{1/2}})_{ij} V_{1/2\mu}^{R\dagger}[\overline{d^c}_i \gamma^\mu P_L L_j] \\ & + (\lambda^R_{\tilde{V}_{1/2}})_{ij} \tilde{V}_{1/2}^{\dagger}[\overline{u^c}_i \gamma^\mu P_L L_j] + (\lambda^L_{V_0})_{ij} V_{0\mu}^{L\dagger}[\overline{Q}_i \gamma^\mu P_L L_j] \\ & + (\lambda^L_{V_{1/2}})_{ij} V_{1/2\mu}^{L\dagger}[\overline{Q^c}_i \gamma^\mu P_R e_j] \\ & + (\lambda^L_{V_1})_{ij} [\overline{Q}_i \gamma^\mu P_L V_{1\mu}^{\dagger} L_j] + \text{H.c.} \end{aligned} \tag{73}$$

for the scalar (S) and vector (V) leptoquarks, respectively. We follow the notation of [114] distinguishing leptoquarks

TABLE V. List of possible scalar and vector leptoquarks and their transformation properties under the Standard Model symmetries [114].

LQ (Ω)	$SU(3)_C$	$SU(2)_L$	$U(1)_Y$	Q
S_0	3	1	$-2/3$	$-1/3$
$\tilde{S}_0$	3	1	$-8/3$	$-4/3$
$S_{1/2}$	$\bar{3}$	2	$-7/3$	$(-2/3, -5/3)$
$\tilde{S}_{1/2}$	$\bar{3}$	2	$-1/3$	$(1/3, -2/3)$
S_1	3	3	$-2/3$	$(2/3, -1/3, -4/3)$
V_0	$\bar{3}$	1	$-4/3$	$-2/3$
$\tilde{V}_0$	$\bar{3}$	1	$-10/3$	$-5/3$
$V_{1/2}$	3	2	$-5/3$	$(-1/3, -4/3)$
$\tilde{V}_{1/2}$	3	2	1/3	$(2/3, -1/3)$
V_1	$\bar{3}$	3	$-4/3$	$(1/3, -2/3, -5/3)$

coupling to left-handed and right-handed quarks. In addition to the LQ-fermion interactions, one can write down the gauge invariant and renormalizable LQ-Higgs interactions,

$$\begin{aligned}\mathcal{L}_{LQ,\Phi} = {} & h^i_{S_0}\tilde{\Phi}^\dagger \tilde{S}_{1/2} S^i_0 + h^i_{V_0}\tilde{\Phi}^\dagger \tilde{V}^\mu_{1/2} V^i_{0\mu} + h_{S_1}\tilde{\Phi}^\dagger S_1 \tilde{S}_{1/2} + h_{V_1}\tilde{\Phi}^\dagger V^\mu_1 \tilde{V}_{1/2\mu} + Y^i_{S_{1/2}}(\tilde{\Phi}^\dagger S^i_{1/2})(\tilde{S}^\dagger_{1/2}\Phi) \\ & + Y^i_{V_{1/2}}(\tilde{\Phi}^\dagger V^{\mu i}_{1/2})(\tilde{V}^\dagger_{1/2\mu}\Phi) + Y_{S_1}(\tilde{\Phi}^\dagger S^\dagger_1 \Phi)\tilde{S}_0 + Y_{V_1}(\tilde{\Phi}^\dagger V^\dagger_{1\mu}\Phi)\tilde{V}^\mu_0 + \kappa^i_S(\Phi^\dagger S_1 \Phi) S^{i\,\dagger}_0 + \kappa^i_V(\Phi^\dagger V^\mu_1 \Phi) V^{i\,\dagger}_{0\mu} + \text{H.c.} \\ & - \sum_\Omega (\eta_\Omega M^2_\Omega - g^{i_1 i_2}_\Omega \Phi^\dagger \Phi)\Omega^{i_1\,\dagger}\Omega^{i_2}, \end{aligned} \tag{74}$$

where the leptoquark triplets are defined as

$$V_1 = \sum_i \tau_i V_{1i} \qquad S_1 = \sum_i \tau_i S_{1i}. \tag{75}$$

These LQ-Higgs interactions are essential when considering contributions to $0\nu\beta\beta$ decay because they result in nonzero correlation functions for, e.g.,

$$\langle S^i_0 \tilde{S}_{1/2}\rangle \propto \sum_{\tilde{I}} \mathcal{N}_{S^i_0 \tilde{I}} \mathcal{N}_{\tilde{S}_{1/2}\tilde{I}}, \tag{76}$$

where $\mathcal{N}$ is the mixing matrix which diagonalizes the mass matrix $\mathcal{N}^T\mathcal{M}^2\mathcal{N} = \mathcal{M}^2_{\text{diag}}$ and $\tilde{I} = \mathcal{N}^T I$ are the mass eigenstate fields. This particular example results in contributions captured by the right diagram in Fig. 16.

After integrating out the heavy LQ degrees of freedom and rearranging the resulting EFT operators via Fierz transformations, one arrives at the effective low-energy four-fermion interactions. The parts of the low-energy Lagrangian relevant for $0\nu\beta\beta$ decay are then given by [114]

$$\begin{aligned}\mathcal{L}_{LQ} = {} & [\bar{e}P_L\nu^c]\left\{\frac{\epsilon_S}{M^2_S}[\bar{u}P_R d] + \frac{\epsilon_V}{M^2_V}[\bar{u}P_L d]\right\} \\ & - [\bar{e}\gamma^\mu P_L \nu^c]\left\{\left(\frac{\alpha^R_S}{M^2_S} + \frac{\alpha^R_V}{M^2_V}\right)[\bar{u}\gamma_\mu P_R d] \right. \\ & \left. - \sqrt{2}\left(\frac{\alpha^L_S}{M^2_S} + \frac{\alpha^L_V}{M^2_V}\right)[\bar{u}\gamma_\mu P_L d]\right\} + \text{H.c.}, \end{aligned} \tag{77}$$

with the low-energy Wilson coefficients

$$\begin{aligned}\epsilon_I = {} & 2^{-\eta_I}[\lambda^L_{I_1}\lambda^R_{\tilde{I}_{1/2}}(\tilde{\theta}^I_{43}(Q^1_I) + \eta_I\sqrt{2}\tilde{\theta}^I_{41}(Q^2_I)) \\ & - \lambda^L_{I_0}\lambda^R_{\tilde{I}_{1/2}}\tilde{\theta}^I_{23}(Q^1_I)] \end{aligned} \tag{78}$$

$$\begin{aligned}\alpha^L_I &= \frac{2}{3+\eta_I}\lambda^L_{I_{1/2}}\lambda^L_{I_1}\tilde{\theta}^I_{24}(Q^2_I), \\ \alpha^R_I &= \frac{2}{r+\eta_I}\lambda^R_{I_0}\lambda^R_{\tilde{I}_{1/2}}\tilde{\theta}^I_{23}(Q^1_I), \end{aligned} \tag{79}$$

where

$$\tilde{\theta}^I_{ij} = \sum_k \mathcal{N}_{ik}\mathcal{N}_{jk}\frac{M^2_I}{M^2_{\tilde{I}_k}}. \tag{80}$$

Here, "common mass scales" M_S and M_V have been inserted for convenience. It should be noted that the exact choice of $M_{S,V}$ does not matter as they drop out. However, the exact LQ masses do enter into the calculation such that for leptoquark masses which are about the same order of magnitude one can choose $M_{S,V}$ to represent the suppression factors. Looking at Eqs. (78) and (79), there is *a priori* no reason from, e.g., naturalness arguments why any of the low energy coefficients α_I and ϵ_I should be suppressed or enhanced compared to the others. However, if the LQ interactions arise from a more complete model or if simply not all possible LQ interactions are realized in nature, hierarchical structures might appear. We will therefore study different settings in which some couplings dominate over the others. From Eq. (77) we can match the Wilson coefficients in Eqs. (78) and (79) onto the LEFT basis arriving at

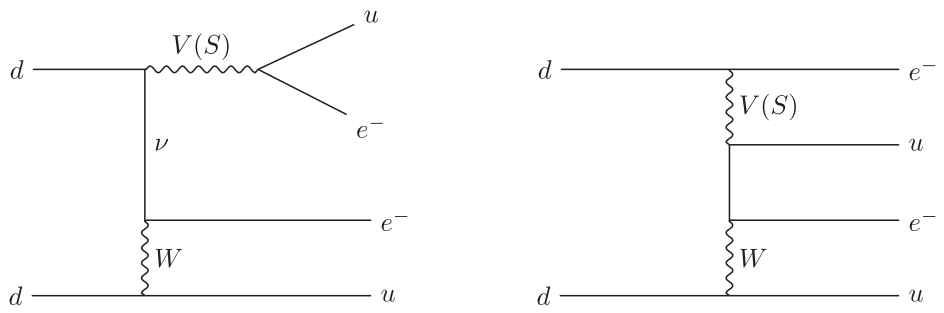

FIG. 16. Feynman diagrams of the vector (V) and scalar (S) leptoquark interactions contributing to $0\nu\beta\beta$.

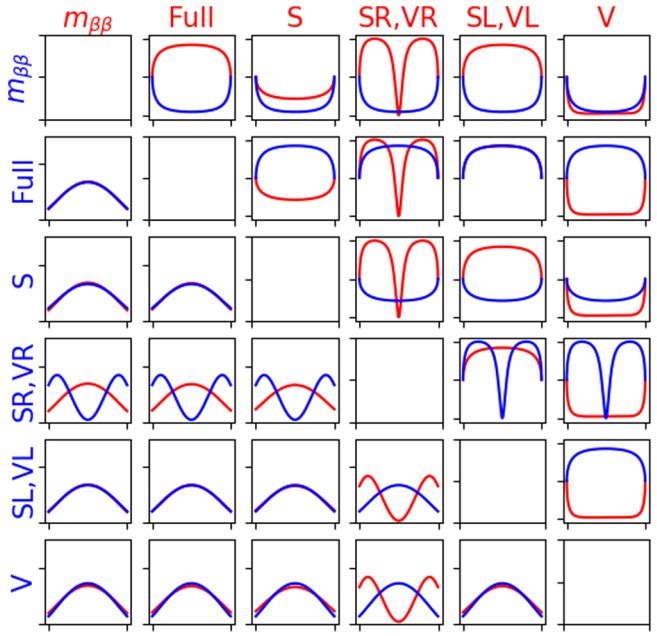

FIG. 17. Angular correlations (upper right) and single electron energy spectra (lower left) resulting from the different LQ contributions as well as the standard mass mechanism in ^{136}Xe. The unknown LECs are set to their order-of-magnitude estimates. The specific choice of the isotope does slightly influence the shape of the angular correlation.

$$
\begin{aligned}
C_{SL}^{(6)} &= \frac{v^2}{M_V^2}\epsilon_V, \\
C_{SR}^{(6)} &= \frac{v^2}{M_S^2}\epsilon_S \\
C_{VL}^{(6)} &= \sqrt{2}v^2\left(\frac{\alpha_S^L}{M_S^2}+\frac{\alpha_V^L}{M_V^2}\right), \\
C_{VR}^{(6)} &= -v^2\left(\frac{\alpha_S^R}{M_S^2}+\frac{\alpha_V^R}{M_V^2}\right).
\end{aligned} \tag{81}
$$

We study the following seven different settings of LQ contributions to $0\nu\beta\beta$ decay:

(1) Full LQ model: $\epsilon_S = \epsilon_V = \alpha_S^L = \alpha_S^R = \alpha_V^L = \alpha_V^R = 1$
(2) Scalar LQs (S): $\epsilon_S = \alpha_S^L = \alpha_S^R = 1$
(3) Scalar LQs coupling to left-handed (LH) fermions (SL): $\alpha_S^L = 1$
(4) Scalar LQs coupling to right-handed (RH) fermions (SR): $\alpha_S^R = 1$
(5) Vector LQs (V): $\epsilon_V = \alpha_V^L = \alpha_V^R = 1$
(6) Vector LQs coupling to LH fermions (VL): $\alpha_V^L = 1$
(7) Vector LQs coupling to RH fermions (VR): $\alpha_V^R = 1$.

The left-handed scalar (SL) and left-handed vector (VL) models result in the same low-energy physics because they match onto the same LEFT operator. The same is true for SR and VR. In Fig. 17 we show the corresponding single electron energy spectra and angular correlations corresponding to each of the above models and compare them with the standard mechanism scenario. When setting the unknown LECs to their order-of-magnitude estimates we find that except for the vector (V) scenario all other models give shapes distinguishable from the standard mass mechanism for at least one phase-space observable. The resulting half-life ratios normalized to the neutrino mass mechanism for each of the above scenarios are shown in Fig. 18. Except for the SR and VR cases, for which the central values suggest somewhat weaker distinguishability, we find that the central values match fairly well the chosen benchmark scenario. Nonetheless, the spread in $R_{im_{\beta\beta}}$ is still significant for the full model as well as the SL and VL models. Considering the central values, the highest ratio when taking ^{76}Ge as the reference isotope is realized in the vector model with $R_{im_{\beta\beta}}^{\max} \sim 4.5$. Again, assuming that the calculated central values of the half-life ratios represent a reasonable estimate, this would correspond to a necessary theoretical accuracy on the nuclear part of the amplitude to satisfy $\frac{\Delta M_{\text{eff}}}{M_{\text{eff}}} \lesssim 19\%$.

In Fig. 19 we show the expected half-lives for the simultaneous realization of the full LQ model and the

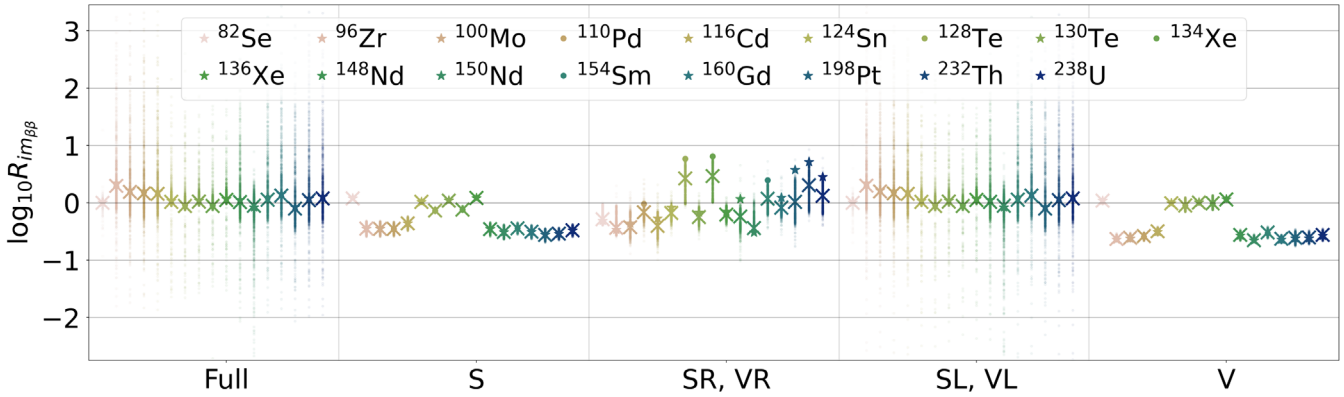

FIG. 18. Half-life ratios resulting from different leptoquark settings when taking ^{76}Ge as the reference isotope. The ratios are compared to the standard mass mechanism.

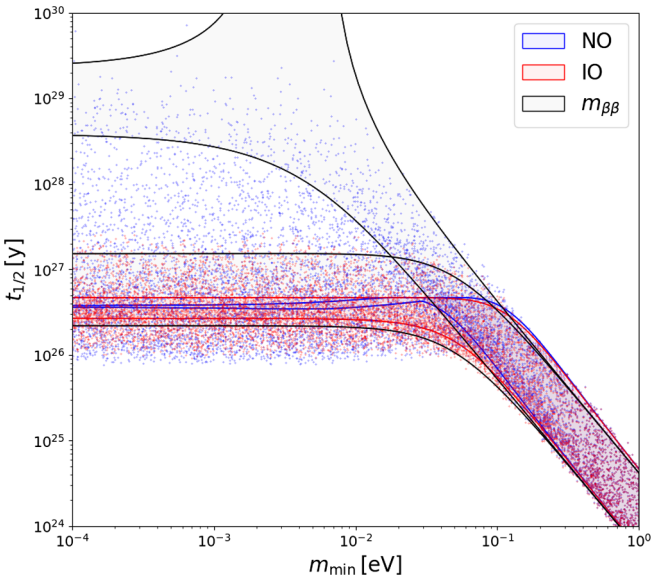

FIG. 19. Here we show the expected half-lives for the full LQ model with the parameters fixed to $\epsilon_S = \epsilon_V = \alpha_S^L = \alpha_S^R = \alpha_V^L = \alpha_V^R = 1$ and the suppression scales $M_S = M_V = 10^7$ GeV.

standard mass mechanism. We assumed the suppression factors to be $M_S = M_V = 10^7$ GeV. One can see that in this setting the inverted mass ordering case is not altered significantly while the half-life in the normal ordering case is decreased such that the gap between the two mass orderings is closed.

V. SUMMARY AND CONCLUSIONS

Neutrinoless double beta decay is the best laboratory probe of lepton number violation and as such can naturally shed light on the generation of neutrino masses as well as associated UV physics. The implications of observation of this hypothetical nuclear process would largely depend on the mechanism responsible for the dominant contribution. In this paper we have performed a detailed analysis discussing the possibilities of experimental discrimination among the 32 different LEFT lepton number violating operators of dimension ≤ 9 triggering $0\nu\beta\beta$ decay at low energy.

The main aim of our study is to understand the differences in various $0\nu\beta\beta$ decay mechanisms and to investigate the possibilities of identifying the potential exotic contribution in experiments. Assuming only one operator at a time, we found that the 32 different LEFT operators can be split into 12 groups which are distinguishable from each other by comparison of ratios of half-lives in different double-beta-decaying isotopes. We calculated the half-life ratios normalized to the standard mass mechanism $R_{im_{\beta\beta}}$ for each of the operator groups discussing the potential for their identification by experimental observations. Varying the currently unknown low-energy constants (LECs) around their order-of-magnitude estimates obtained using NDA we observed that their impact on the expected half-life ratios can be significant for most operator groups. To quantify this impact and temporarily eliminate it in our conclusions we focused on two different scenarios; namely, we identified the central values of the ratio ranges as well as the worst-case scenario considering the value of the ratios closest to 1 within each ratio range. In Fig. 8 we summarized the potential of distinguishing among different operator groups for both of these scenarios considering all isotopes for which the experimental limit on $0\nu\beta\beta$ decay half-life exists. Based on the central-value scenario we estimated the required theoretical accuracy on the nuclear physics calculations, parametrized by an effective nuclear matrix element M_{eff}, which would allow for identifying nonstandard mechanisms in the single operator dominance scenario. We found that identifying all the nonstandard mechanisms via half-life ratios would require (at least) a few-percent accuracy. While the required accuracy of the theoretical description is beyond the current status of nuclear uncertainties, advances in *ab initio* calculations of nuclear matrix elements may be able to deliver such precision in the future provided that the currently unknown LECs are fixed with similar accuracy as those that are already under control.

The additional information that can be inferred from the phase-space observables does not allow for distinguishing operators within the 12 operator groups corresponding to distinct half-life ratios. However, the phase-space observables are much less affected by nuclear uncertainties such that they can potentially deliver important insight into the underlying mechanism of $0\nu\beta\beta$ decay even if nuclear uncertainties remain significant. For operator groups such as $C_V(9)$ or $\tilde{C}_V(9)$ for which the expected half-life ratios do not differ significantly from the standard mass mechanism measurements, tracking the outgoing electrons would be a more promising approach of identification even if nuclear uncertainties are substantially reduced. Therefore, future experiments that would have the required technology such as SuperNEMO seem to be very relevant. The operator groups that could be distinguished by means of phase-space observables are also marked in Fig. 8.

Besides the effective approach detailing individual operators, we focused also on $0\nu\beta\beta$ decay contributions triggered by three different high-energy models. In each case, we identified and discussed the signatures that could help to distinguish these models in observations of $0\nu\beta\beta$ decay. Our approach can be easily extended to any other UV model that can be matched onto the applied EFT framework.

Based on the obtained results and following their discussion it becomes clear that, although it might be possible to unravel an exotic contribution to $0\nu\beta\beta$ decay, pinpointing the dominant mechanism underlying this hypothetical nuclear process most probably would not be possible without other, complementary experiments. As discussed, the possibilities of employing different double-beta processes seems to be rather unlikely because of their

phase-space suppression. On the other hand, the underlying mechanism could be identified by combining the $0\nu\beta\beta$ decay data with different experiments searching for lepton number violation, such as meson decays, tau decays, or collider searches, which can, however, more naturally verify a complete UV scenario rather than a specific effective operator. Useful information will be provided also by measurements aiming to determine the absolute neutrino mass scale, including the CMB data providing a constraint on the sum of neutrino masses, $\sum_i m_{\nu_i}$. A detailed discussion of the interplay with complementary probes of neutrino masses and lepton number (non)conservation is however beyond the scope of this paper. Similarly, we have not covered the possibility of existence of light sterile neutrinos and its implications for $0\nu\beta\beta$ decay. The same methods as employed in this study may allow to unravel additional contributions to $0\nu\beta\beta$ decay induced by light sterile neutrinos.

ACKNOWLEDGMENTS

We would like to thank Jordy de Vries for many fruitful discussions and useful comments. We are also grateful to Frank F. Deppisch for valuable comments on the final version of the manuscript. L. G. acknowledges support from the National Science Foundation, Grant No. PHY-1630782, and to the Heising-Simons Foundation, Grant No. 2017-228.

APPENDIX A: DOUBLE-β MODES

In Table VI we present a list of all naturally occurring isotopes that decay via any of the $0\nu\beta\beta$ modes, i.e., $0\nu\beta^-\beta^-, 0\nu\beta^+\beta^+, 0\nu\mathrm{EC}\beta^+$ and 0νECEC. The isotopes as well as the corresponding Q values are taken and calculated from the NIST list of elements [94].

TABLE VI. Complete list of natural double-β elements and the corresponding Q values calculated from the NIST list of elements [94] using the conditions (35), (37), (39) and (41). Overall there are 69 different natural elements that can decay via at least one double-β mode.

$2\nu\beta^-\beta^-$		$2\nu\beta^+\beta^+$		$2\nu\mathrm{EC}\beta^+$		2νECEC	
^{A}Z	Q [MeV]	^{A}Z	Q [MeV]	^{A}Z	Q [MeV]	^{A}Z	Q [MeV]
^{46}Ca	0.99	^{78}Kr	0.80	^{50}Cr	0.15	^{36}Ar	0.43
^{48}Ca	4.27	^{96}Ru	0.67	^{58}Ni	0.90	^{40}Ca	0.19
^{70}Zn	1.00	^{106}Cd	0.73	^{64}Zn	0.073	^{50}Cr	1.17
^{76}Ge	2.04	^{124}Xe	0.82	^{74}Se	0.19	^{54}Fe	0.68
^{80}Se	0.13	^{130}Ba	0.57	^{78}Kr	1.82	^{58}Ni	1.93
^{82}Se	3.00	^{136}Ce	0.33	^{84}Sr	0.77	^{64}Zn	1.09
^{86}Kr	1.26			^{92}Mo	0.63	^{74}Se	1.21
^{94}Zr	1.14			^{96}Ru	1.69	^{78}Kr	2.85
^{96}Zr	3.35			^{102}Pd	0.15	^{84}Sr	1.79
^{98}Mo	0.11			^{106}Cd	1.75	^{92}Mo	1.65
^{100}Mo	3.03			^{112}Sn	0.90	^{96}Ru	2.71
^{104}Ru	1.30			^{120}Te	0.71	^{102}Pd	1.17
^{110}Pd	2.02			^{124}Xe	1.84	^{106}Cd	2.78
^{114}Cd	0.54			^{130}Ba	1.60	^{108}Cd	0.27
^{116}Cd	2.81			^{136}Ce	1.36	^{112}Sn	1.92
^{122}Sn	0.37			^{144}Sm	0.76	^{120}Te	1.73
^{124}Sn	2.29			^{156}Dy	0.98	^{124}Xe	2.86
^{128}Te	0.87			^{162}Er	0.82	^{126}Xe	0.92
^{130}Te	2.53			^{168}Yb	0.39	^{130}Ba	2.62
^{134}Xe	0.83			^{174}Hf	0.077	^{132}Ba	0.84
^{136}Xe	2.46			^{184}Os	0.43	^{136}Ce	2.38
^{142}Ce	1.42			^{190}Pt	0.36	^{138}Ce	0.69
^{146}Nd	0.070					^{144}Sm	1.78
^{148}Nd	1.93					^{152}Gd	0.056
^{150}Nd	3.37					^{156}Dy	2.01
^{154}Sm	1.25					^{158}Dy	0.28
^{160}Gd	1.73					^{162}Er	1.85
^{170}Er	0.66					^{164}Er	0.025
^{176}Yb	1.09					^{168}Yb	1.41

(Table continued)

TABLE VI. *(Continued)*

$2\nu\beta^-\beta^-$		$2\nu\beta^+\beta^+$		$2\nu\mathrm{EC}\beta^+$		$2\nu\mathrm{ECEC}$	
${}^AZ$	Q [MeV]	${}^AZ$	Q [MeV]	${}^AZ$	Q [MeV]	${}^AZ$	Q [MeV]
${}^{186}\mathrm{W}$	0.49					${}^{174}\mathrm{Hf}$	1.10
${}^{192}\mathrm{Os}$	0.41					${}^{180}\mathrm{W}$	0.14
${}^{198}\mathrm{Pt}$	1.05					${}^{184}\mathrm{Os}$	1.45
${}^{204}\mathrm{Hg}$	0.42					${}^{190}\mathrm{Pt}$	1.38
${}^{232}\mathrm{Th}$	0.84					${}^{196}\mathrm{Hg}$	0.82
${}^{238}\mathrm{U}$	1.14						

APPENDIX B: CONTRIBUTIONS FROM EACH OPERATOR

Assuming only one nonvanishing operator at a time, the half-life can be written in terms of a single Wilson coefficient, different phase-space factors and the nuclear contributions determined by the different NMEs and LECs. For convenience, we list the explicit decay rate equations for each operator below:

$$m_{\beta\beta}\colon\ T_{1/2}^{-1} = g_A^4 |m_{\beta\beta}|^2 G_{01} \left| \frac{V_{ud}^2}{m_e} \left(\frac{1}{g_A^2} M_F - M_{GT} - 2\frac{m_\pi^2 \mathbf{g_\nu^{NN}}}{g_A^2} M_{F,sd} \right) \right|^2 \tag{B1}$$

$$\begin{aligned} C_{VL}^{(6)}\colon\ T_{1/2}^{-1} = g_A^4 |C_{VL}^{(6)}|^2 \Bigg\{ & 4G_{02} \left| \frac{V_{ud}}{3} \left(\frac{g_V^2}{g_A^2} M_F + \frac{1}{3}(2M_{GT}^{AA} + M_T^{AA}) + \frac{6\mathbf{g_{VL}^E}}{g_A^2} M_{F,sd} \right) \right|^2 \\ & + 2G_{04} \left| \frac{V_{ud}}{6} \left(\frac{g_V^2}{g_A^2} M_F - \frac{1}{3}(M_{GT}^{AA} - 4M_T^{AA}) - 3(M_{GT}^{AP} + M_{GT}^{PP} + M_T^{AP} + M_T^{PP}) - \frac{12\mathbf{g_{VL}^{m_e}}}{g_A^2} M_{F,sd} \right) \right|^2 \\ & - 4G_{03}\mathrm{Re}\Bigg[\frac{|V_{ud}|^2}{18} \left(\frac{g_V^2}{g_A^2} M_F + \frac{1}{3}(2M_{GT}^{AA} + M_T^{AA}) + \frac{6\mathbf{g_{VL}^E}}{g_A^2} M_{F,sd} \right)^* \\ & \times \left(\frac{g_V^2}{g_A^2} M_F - \frac{1}{3}(M_{GT}^{AA} - 4M_T^{AA}) - 3(M_{GT}^{AP} + M_{GT}^{PP} + M_T^{AP} + M_T^{PP}) - \frac{12\mathbf{g_{VL}^{m_e}}}{g_A^2} M_{F,sd} \right) \Bigg] \\ & + G_{09} \left| \frac{m_N}{m_e} V_{ud} \left[2\frac{g_A}{g_M}(M_{GT}^{MM} + M_T^{MM}) + \frac{m_\pi^2}{m_N^2} \left(-\frac{2}{g_A^2} \mathbf{g_{VL}^{NN}} M_{F,sd} + \frac{1}{2} \mathbf{g_{VL}^{\pi N}} (M_{GT,sd}^{AP} + M_{T,sd}^{AP}) \right) \right] \right|^2 \Bigg\} \end{aligned} \tag{B2}$$

$$\begin{aligned} C_{VR}^{(6)}\colon\ T_{1/2}^{-1} = g_A^4 |C_{VR}^{(6)}|^2 \Bigg\{ & 4G_{02} \left| \frac{V_{ud}}{3} \left(\frac{g_V^2}{g_A^2} M_F - \frac{1}{3}(2M_{GT}^{AA} + M_T^{AA}) + 6\frac{\mathbf{g_{VR}^E}}{g_A^2} M_{F,sd} \right) \right|^2 \\ & + 2G_{04} \left| \frac{V_{ud}}{6} \left(\frac{g_V^2}{g_A^2} M_F + \frac{1}{3}(M_{GT}^{AA} - 4M_T^{AA}) + 3(M_{GT}^{AP} + M_{GT}^{PP} + M_T^{AP} + M_T^{PP}) - 12\frac{\mathbf{g_{VR}^{me}}}{g_A^2} M_{F,sd} \right) \right|^2 \\ & + 2G_{03}\mathrm{Re}\Bigg[\frac{|V_{ud}|^2}{18} \left(\frac{g_V^2}{g_A^2} M_F - \frac{1}{3}(2M_{GT}^{AA} + M_T^{AA}) + 6\frac{\mathbf{g_{VR}^E}}{g_A^2} M_{F,sd} \right)^* \\ & \times \left(\frac{g_V^2}{g_A^2} M_F + \frac{1}{3}(M_{GT}^{AA} - 4M_T^{AA}) + 3(M_{GT}^{AP} + M_{GT}^{PP} + M_T^{AP} + M_T^{PP}) - 12\frac{\mathbf{g_{VR}^{m_e}}}{g_A^2} M_{F,sd} \right) \Bigg] \Bigg\} \end{aligned} \tag{B3}$$

$$C_{SL,SR}^{(6)}\colon\ T_{1/2}^{-1} = g_A^4 |C_{SL,SR}^{(6)}|^2 G_{01} \left| \frac{B}{m_e} V_{ud} M_{PS} \right|^2 \tag{B4}$$

$$C_T^{(6)}\colon\ T_{1/2}^{-1} = g_A^4 |C_T^{(6)}|^2 G_{01} \left| V_{ud} \left[2\frac{\mathbf{g_T'} - \mathbf{g_T^{NN}}}{g_A^2} \frac{m_\pi^2}{m_N^2} M_{F,sd} - \frac{8g_T}{g_M}(M_{GT}^{MM} + M_T^{MM}) \right] \right|^2 \tag{B5}$$

$$C_{VL,VR}^{(7)}\colon\ T_{1/2}^{-1} = g_A^4 |C_{VL,VR}^{(7)}|^2 G_{01} \left| \frac{m_\pi^2}{m_e v} V_{ud} M_{PS} \right|^2 \tag{B6}$$

$$C^{(9)}_{1L,1R}(')\colon\ T^{-1}_{1/2} = g_A^4 |C^{(9)}_{1L,1R}(')|^2 G_{01} \left| \frac{5 g_1^{\pi\pi}}{6 m_N^2} \left(\frac{1}{2} M^{AP}_{GT,sd} + M^{PP}_{GT,sd} + \frac{1}{2} M^{AP}_{T,sd} + M^{PP}_{T,sd} \right) + \left(\mathbf{g_1^{\pi N}} - \frac{5}{6} g_1^{\pi\pi} \right) \frac{m_\pi^2}{2 m_N^2} (M^{AP}_{GT,sd} + M^{AP}_{T,sd}) - 2 \frac{\mathbf{g_1^{NN}}}{g_A^2} \frac{m_\pi^2}{m_N^2} M_{F,sd} \right|^2 \tag{B7}$$

$$C^{(9)}_{2,3\cdot L,R}(')\colon\ T^{-1}_{1/2} = g_A^4 |C^{(9)}_{2,3\cdot L,R}(')|^2 G_{01} \left| \frac{5 g_{2,3}^{\pi\pi}}{6 m_N^2} \left(\frac{1}{2} M^{AP}_{GT,sd} + M^{PP}_{GT,sd} + \frac{1}{2} M^{AP}_{T,sd} + M^{PP}_{T,sd} \right) + 2 \frac{\mathbf{g_{2,3}^{NN}}}{g_A^2} \frac{m_\pi^2}{m_N^2} M_{F,sd} \right| \tag{B8}$$

$$C^{(9)}_{4,5\cdot L,R}\colon\ T^{-1}_{1/2} = g_A^4 |C^{(9)}_{4,5\cdot L,R}|^2 G_{01} \left| \frac{5 g_{4,5}^{\pi\pi}}{6 m_N^2} \left(\frac{1}{2} M^{AP}_{GT,sd} + M^{PP}_{GT,sd} + \frac{1}{2} M^{AP}_{T,sd} + M^{PP}_{T,sd} \right) - 2 \frac{\mathbf{g_{4,5}^{NN}}}{g_A^2} \frac{m_\pi^2}{m_N^2} M_{F,sd} \right| \tag{B9}$$

$$C^{(9)}_{V}\colon\ T^{-1}_{1/2} = g_A^4 |C^{(9)}_{V}|^2 G_{09} \left| \frac{m_\pi^2}{m_e v} \left(-\frac{2}{g_A} \mathbf{g_6^{NN}} M_{F,sd} + \frac{1}{2} \mathbf{g_V^{\pi N}} (M^{AP}_{GT,sd} + M^{AP}_{T,sd}) \right) \right|^2 \tag{B10}$$

$$\tilde{C}^{(9)}_{V}\colon\ T^{-1}_{1/2} = g_A^4 |\tilde{C}^{(9)}_{V}|^2 G_{09} \left| \frac{m_\pi^2}{m_e v} \left(-\frac{2}{g_A} \mathbf{g_7^{NN}} M_{F,sd} + \frac{1}{2} \mathbf{\tilde{g}_V^{\pi N}} (M^{AP}_{GT,sd} + M^{AP}_{T,sd}) \right) \right|^2 . \tag{B11}$$

APPENDIX C: CONSIDERING ALL ISOTOPES

While we have focused our discussion on isotopes for which experimental limits on the half-lives exist, we want to present our main findings of Fig. 8 here again but now considering all naturally occurring $0\nu\beta\beta$ isotopes for which we have nuclear matrix elements available in the IBM2 framework. The corresponding results are presented in Fig. 20. In Figs. 21 and 22 we show the resulting ratios including variations of the unknown LECs similar to Figs. 5 and 6 when considering the whole set of isotopes available.

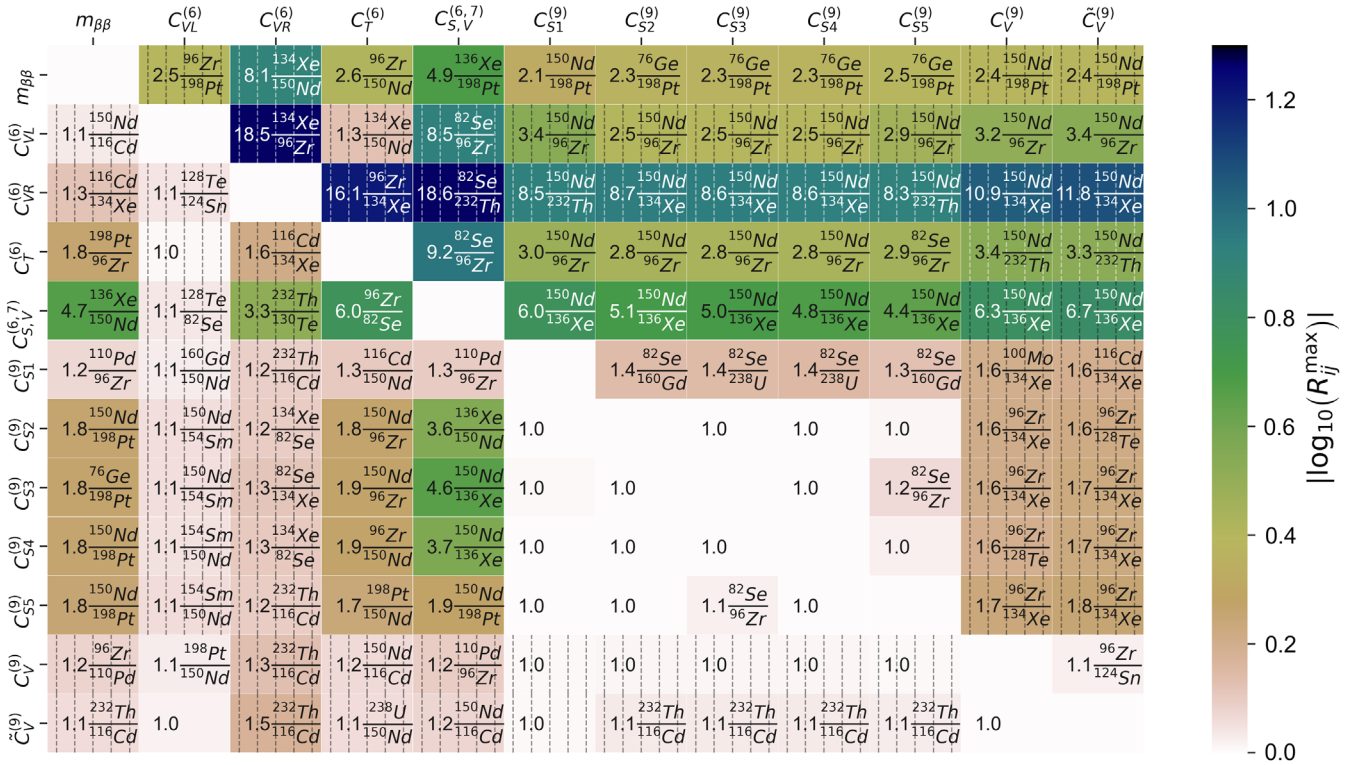

FIG. 20. Same as Fig. 8 but now for all isotopes with available NMEs in the IBM2 framework: The maximal ratios $R^{\max}_{ij}$ for all operator combinations i, j are shown. The exact values and the corresponding isotopes are displayed in each tile. Additionally, operator combinations that result in different phase-space observables are marked by dashed-line shading. In the upper right half of the plot we show the ratios considering the central values from the variation of the LECs. In the lower left half we show the worst-case scenario considering the values of ratios R_{ij} that are closest to 1 within the range obtained by the variation of the LECs.

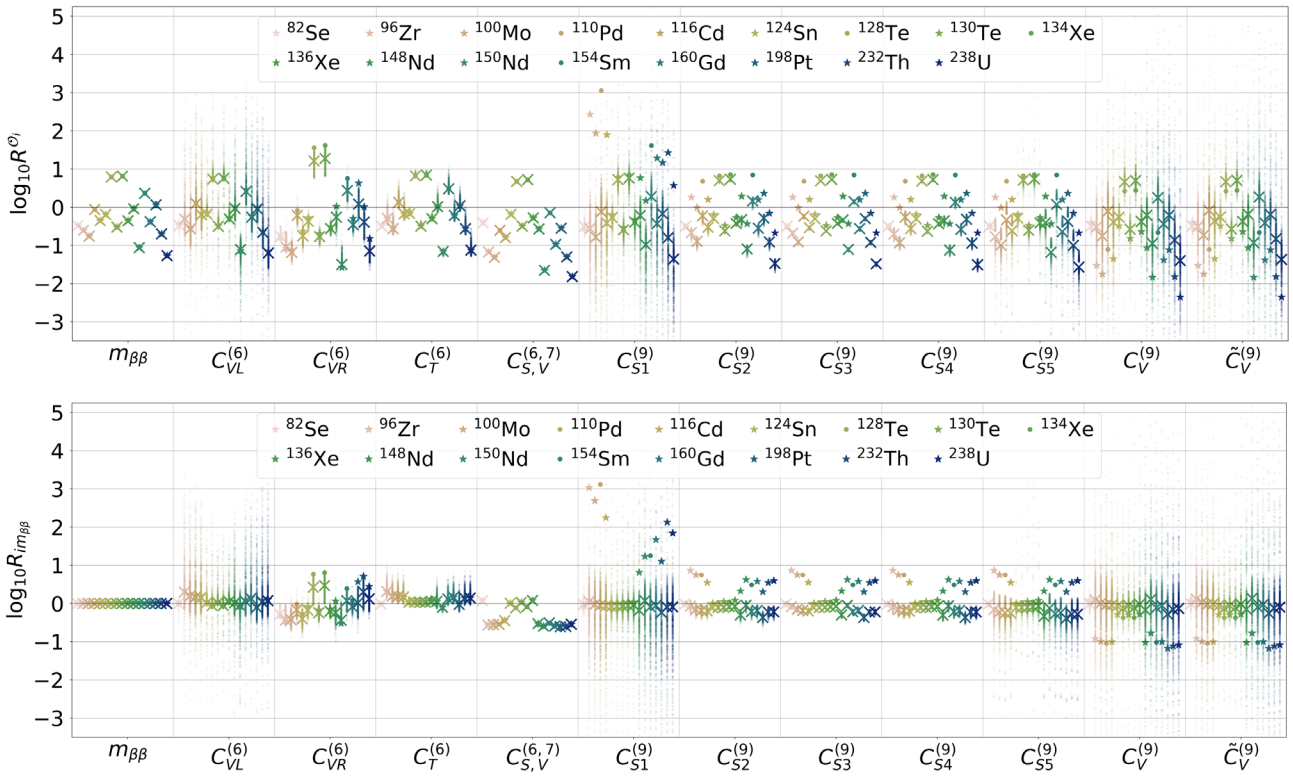

FIG. 21. The decay rate ratios R^{O_i} (upper plot) and $R_{im_{\beta\beta}}$ (lower plot) for the different operator groups are shown. The larger markers represent the choice of vanishing unknown LECs with $g_{6,7}^{NN} = g_V^{\pi N} = \tilde{g}_V^{\pi N} = 1$. Isotopes with a PSF $G_0 > 10^{-14}$ y^{-1} are represented by stars while isotopes with smaller PSFs are represented by round markers. The additional points represent variations of the different unknown LECs g_i randomly chosen from $[-\sqrt{10}, -1/\sqrt{10}] \times |g_i|$ and $[+1/\sqrt{10}, +\sqrt{10}] \times |g_i|$ except for g_ν^{NN} which is varied in a range of $\pm 50\%$. The crosses represent the central values of the variation, i.e., the median values. The reference isotope is chosen to be ^{76}Ge.

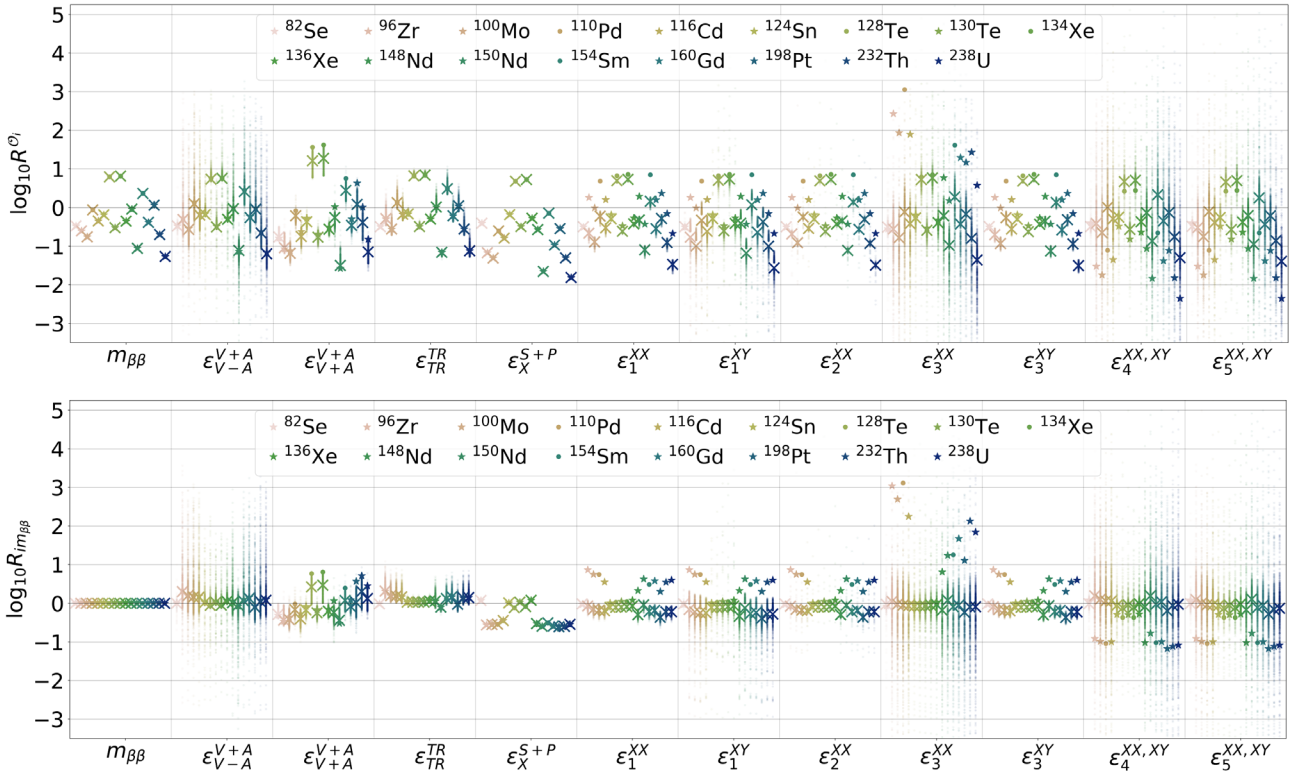

FIG. 22. The decay rate ratios R^{O_i} (upper plot) and $R_{im_{\beta\beta}}$ (lower plot) for the different operator groups in the ϵ *basis*.

[1] W. Furry, On transition probabilities in double beta-disintegration, Phys. Rev. **56**, 1184 (1939).

[2] J. Schechter and J. W. F. Valle, Neutrinoless double-β decay in $SU(2) \times U(1)$ theories, Phys. Rev. D **25**, 2951 (1982).

[3] H. Pas, M. Hirsch, H. Klapdor-Kleingrothaus, and S. Kovalenko, Towards a superformula for neutrinoless double beta decay, Phys. Lett. B **453**, 194 (1999).

[4] H. Pas, M. Hirsch, H. Klapdor-Kleingrothaus, and S. Kovalenko, A superformula for neutrinoless double beta decay. 2. The short range part, Phys. Lett. B **498**, 35 (2001).

[5] K. S. Babu and C. N. Leung, Classification of effective neutrino mass operators, Nucl. Phys. **B619**, 667 (2001).

[6] A. de Gouvea and J. Jenkins, A survey of lepton number violation via effective operators, Phys. Rev. D **77**, 013008 (2008).

[7] F. Bonnet, M. Hirsch, T. Ota, and W. Winter, Systematic decomposition of the neutrinoless double beta decay operator, J. High Energy Phys. 03 (2013) 055; Erratum, J. High Energy Phys. 04 (2014) 090.

[8] F. F. Deppisch, M. Hirsch, and H. Päs, Neutrinoless double beta decay and physics beyond the standard model, J. Phys. G **39**, 124007 (2012).

[9] V. Cirigliano, W. Dekens, J. de Vries, M. L. Graesser, and E. Mereghetti, Neutrinoless double beta decay in chiral effective field theory: Lepton number violation at dimension seven, J. High Energy Phys. 12 (2017) 082.

[10] V. Cirigliano, W. Dekens, J. de Vries, M. L. Graesser, and E. Mereghetti, A neutrinoless double beta decay master formula from effective field theory, J. High Energy Phys. 12 (2018) 097.

[11] L. Graf, F. F. Deppisch, F. Iachello, and J. Kotila, Short-range neutrinoless double beta decay mechanisms, Phys. Rev. D **98**, 095023 (2018).

[12] F. F. Deppisch, L. Graf, F. Iachello, and J. Kotila, Analysis of light neutrino exchange and short-range mechanisms in $0\nu\beta\beta$ decay, Phys. Rev. D **102**, 095016 (2020).

[13] J. Kotila, J. Ferretti, and F. Iachello, Long-range neutrinoless double beta decay mechanisms, arXiv:2110.09141.

[14] J. C. Pati and A. Salam, Lepton number as the fourth color, Phys. Rev. D **10**, 275 (1974); Erratum, Phys. Rev. D **11**, 703 (1975).

[15] R. N. Mohapatra and J. C. Pati, Left-right gauge symmetry and an isoconjugate model of *CP* violation, Phys. Rev. D **11**, 566 (1975).

[16] R. N. Mohapatra and J. C. Pati, A natural left-right symmetry, Phys. Rev. D **11**, 2558 (1975).

[17] G. Senjanovic and R. N. Mohapatra, Exact left-right symmetry and spontaneous violation of parity, Phys. Rev. D **12**, 1502 (1975).

[18] W.-C. Huang and J. Lopez-Pavon, On neutrinoless double beta decay in the minimal left-right symmetric model, Eur. Phys. J. C **74**, 2853 (2014).

[19] C. Giunti and M. Laveder, Short-baseline electron neutrino disappearance, tritium beta decay and neutrinoless double-beta decay, Phys. Rev. D **82**, 053005 (2010).

[20] J. Barry, W. Rodejohann, and H. Zhang, Light sterile neutrinos: Models and phenomenology, J. High Energy Phys. 07 (2011) 091.

[21] J. Barea, J. Kotila, and F. Iachello, Limits on sterile neutrino contributions to neutrinoless double beta decay, Phys. Rev. D **92**, 093001 (2015).

[22] W. Dekens, J. de Vries, K. Fuyuto, E. Mereghetti, and G. Zhou, Sterile neutrinos and neutrinoless double beta decay in effective field theory, J. High Energy Phys. 06 (2020) 097.

[23] G. Li, M. J. Ramsey-Musolf, and J. C. Vasquez, Left-Right Symmetry and Leading Contributions to Neutrinoless Double Beta Decay, Phys. Rev. Lett. **126**, 151801 (2021).

[24] P. D. Bolton, F. F. Deppisch, and P. S. Bhupal Dev, Neutrinoless double beta decay versus other probes of heavy sterile neutrinos, J. High Energy Phys. 03 (2020) 170.

[25] M. Agostini, G. R. Araujo, A. M. Bakalyarov, M. Balata, I. Barabanov, L. Baudis *et al.* (GERDA Collaboration), Final Results of Gerda on the Search for Neutrinoless Double-β Decay, Phys. Rev. Lett. **125**, 252502 (2020).

[26] O. Azzolini, J. W. Beeman, F. Bellini, M. Beretta, M. Biassoni, C. Brofferio *et al.*, Final Result of CUPID-0 Phase-I in the Search for the ^{82}Se Neutrinoless Double-β Decay, Phys. Rev. Lett. **123**, 032501 (2019).

[27] J. Argyriades *et al.*, Measurement of the two neutrino double beta decay half-life of Zr-96 with the NEMO-3 detector, Nucl. Phys. **A847**, 168 (2010).

[28] E. Armengaud, C. Augier, A. S. Barabash, F. Bellini, G. Benato, A. Benoît *et al.* (CUPID-Mo Collaboration), New Limit for Neutrinoless Double-Beta Decay of ^{100}Mo from the CUPID-Mo Experiment, Phys. Rev. Lett. **126**, 181802 (2021).

[29] F. A. Danevich *et al.*, Search for double beta decay of ^{116}Cd with enriched $^{116}CdWO_4$ crystal scintillators (aurora experiment), J. Phys. Conf. Ser. **718**, 062009 (2016).

[30] C. Arnaboldi *et al.*, A calorimetric search on double beta decay of ^{130}Te, Phys. Lett. B **557**, 167 (2003).

[31] D. Q. Adams, C. Alduino, K. Alfonso, F. T. Avignone, O. Azzolini, G. Bari *et al.* (CUORE Collaboration), Improved Limit on Neutrinoless Double-Beta Decay in ^{130}Te with CUORE, Phys. Rev. Lett. **124**, 122501 (2020).

[32] G. Anton, I. Badhrees, P. S. Barbeau, D. Beck, V. Belov, T. Bhatta *et al.* (EXO-200 Collaboration), Search for Neutrinoless Double-β Decay with the Complete EXO-200 Dataset, Phys. Rev. Lett. **123**, 161802 (2019).

[33] A. Gando, Y. Gando, T. Hachiya, A. Hayashi, S. Hayashida, H. Ikeda *et al.* (KamLAND-Zen Collaboration), Search for Majorana Neutrinos Near the Inverted Mass Hierarchy Region with KamLAND-Zen, Phys. Rev. Lett. **117**, 082503 (2016).

[34] J. Argyriades *et al.*, Measurement of the double-β decay half-life of ^{150}Nd and search for neutrinoless decay modes with the NEMO-3 detector, Phys. Rev. C **80**, 032501(R) (2009).

[35] S. Abe *et al.* (KamLAND-Zen Collaboration), First search for the Majorana nature of neutrinos in the inverted mass ordering region with KamLAND-Zen, arXiv:2203.02139.

[36] N. Abgrall *et al.*, The large enriched germanium experiment for neutrinoless double beta decay (legend), AIP Conf. Proc. **1894**, 020027 (2017).

[37] N. Abgrall *et al.* (LEGEND Collaboration), The large enriched germanium experiment for neutrinoless $\beta\beta$ decay: LEGEND-1000 preconceptual design report, arXiv:2107.11462.
[38] E. Armengaud *et al.*, The CUPID-Mo experiment for neutrinoless double-beta decay: Performance and prospects, Eur. Phys. J. C **80**, 44 (2020).
[39] V. Albanese *et al.*, The SNO + experiment, J. Instrum. **16**, P08059 (2021).
[40] G. Adhikari *et al.* (nEXO Collaboration), nEXO: Neutrinoless double beta decay search beyond 10^{28} year half-life sensitivity, J. Phys. G **49**, 015104 (2022).
[41] F. F. Deppisch, L. Graf, and F. Šimkovic, Searching for New Physics in Two-Neutrino Double Beta Decay, Phys. Rev. Lett. **125**, 171801 (2020).
[42] M. J. Dolinski, A. W. Poon, and W. Rodejohann, Neutrinoless double-beta decay: Status and prospects, Annu. Rev. Nucl. Part. Sci. **69**, 219 (2019).
[43] M. Agostini, G. Benato, J. A. Detwiler, J. Menéndez, and F. Vissani, Toward the discovery of matter creation with neutrinoless double-beta decay, arXiv:2202.01787.
[44] V. Cirigliano *et al.*, Neutrinoless double-beta decay: A roadmap for matching theory to experiment, arXiv:2203.12169.
[45] J. de Vries, L. Gráf, and O. Scholer (to be published).
[46] M. L. Graesser, An electroweak basis for neutrinoless double β decay, J. High Energy Phys. 08 (2017) 099.
[47] G. Prezeau, M. J. Ramsey-Musolf, and P. Vogel, Neutrinoless double beta decay and effective field theory, Phys. Rev. D **68**, 034016 (2003).
[48] S. Weinberg, Baryon- and Lepton-Nonconserving Processes, Phys. Rev. Lett. **43**, 1566 (1979).
[49] T. Bhattacharya, V. Cirigliano, S. D. Cohen, R. Gupta, H.-W. Lin, and B. Yoon (Precision Neutron Decay Matrix Elements (PNDME) Collaboration), Axial, scalar, and tensor charges of the nucleon from $2 + 1 + 1$-flavor lattice QCD, Phys. Rev. D **94**, 054508 (2016).
[50] A. Nicholson, E. Berkowitz, H. Monge-Camacho, D. Brantley, N. Garron, C. C. Chang *et al.*, Heavy Physics Contributions to Neutrinoless Double Beta Decay from QCD, Phys. Rev. Lett. **121**, 172501 (2018).
[51] V. Cirigliano, W. Dekens, J. de Vries, M. Hoferichter, and E. Mereghetti, Toward Complete Leading-Order Predictions for Neutrinoless Double β Decay, Phys. Rev. Lett. **126**, 172002 (2021).
[52] V. Cirigliano, W. Dekens, J. de Vries, M. Hoferichter, and E. Mereghetti, Determining the leading-order contact term in neutrinoless double β decay, J. High Energy Phys. 05 (2021) 289.
[53] R. Wirth, J. M. Yao, and H. Hergert, Ab Initio Calculation of the Contact Operator Contribution in the Standard Mechanism for Neutrinoless Double Beta Decay, Phys. Rev. Lett. **127**, 242502 (2021).
[54] V. Cirigliano, W. Dekens, J. de Vries, M. L. Graesser, E. Mereghetti, S. Pastore, and U. van Kolck, New Leading Contribution to Neutrinoless Double-β Decay, Phys. Rev. Lett. **120**, 202001 (2018).
[55] V. Cirigliano, W. Dekens, J. de Vries, M. L. Graesser, E. Mereghetti, S. Pastore, M. Piarulli, U. van Kolck, and R. B. Wiringa, Renormalized approach to neutrinoless double- β decay, Phys. Rev. C **100**, 055504 (2019).
[56] G. Li, M. J. Ramsey-Musolf, S. Su, and J. C. Vasquez, Lepton number violation: From $0\nu\beta\beta$ decay to long-lived particle searches, Phys. Rev. D **105**, 115018 (2022).
[57] M. L. Graesser, G. Li, M. J. Ramsey-Musolf, T. Shen, and S. Urrutia-Quiroga, Uncovering a chirally suppressed mechanism of $0\nu\beta\beta$ decay with LHC searches, arXiv:2202.01237.
[58] R. Arnold *et al.*, Measurement of the $2\nu\beta\beta$ decay half-life and search for the $0\nu\beta\beta$ decay of ^{116}Cd with the NEMO-3 detector, Phys. Rev. D **95**, 012007 (2017).
[59] R. Arnold *et al.*, Probing new physics models of neutrinoless double beta decay with supernemo, Eur. Phys. J. C **70**, 927 (2010).
[60] J. Kotila and F. Iachello, Phase-space factors for double-β decay, Phys. Rev. C **85**, 034316 (2012).
[61] D. c. v. Štefánik, R. Dvornický, F. Šimkovic, and P. Vogel, Reexamining the light neutrino exchange mechanism of the $0\nu\beta\beta$ decay with left- and right-handed leptonic and hadronic currents, Phys. Rev. C **92**, 055502 (2015).
[62] A. Ali, A. V. Borisov, and D. V. Zhuridov, Probing new physics in the neutrinoless double beta decay using electron angular correlation, Phys. Rev. D **76**, 093009 (2007).
[63] F. Deppisch and H. Päs, Pinning Down the Mechanism of Neutrinoless Double β Decay with Measurements in Different Nuclei, Phys. Rev. Lett. **98**, 232501 (2007).
[64] V. M. Gehman and S. R. Elliott, Multiple-isotope comparison for determining $0\nu\beta\beta$ mechanisms, J. Phys. G **34**, 667 (2007); Erratum, J. Phys. G **35**, 029701 (2008).
[65] E. Lisi, A. M. Rotunno, and F. Šimkovic, Degeneracies of particle and nuclear physics uncertainties in neutrinoless $\beta\beta$ decay, Phys. Rev. D **92**, 093004 (2015).
[66] G. L. Fogli, E. Lisi, and A. M. Rotunno, Probing particle and nuclear physics models of neutrinoless double beta decay with different nuclei, Phys. Rev. D **80**, 015024 (2009).
[67] F. Simkovic, J. Vergados, and A. Faessler, Few active mechanisms of the neutrinoless double beta-decay and effective mass of Majorana neutrinos, Phys. Rev. D **82**, 113015 (2010).
[68] A. Meroni, S. T. Petcov, and F. Simkovic, Multiple *CP* non-conserving mechanisms of $(\beta\beta)_{0\nu}$-decay and nuclei with largely different nuclear matrix elements, J. High Energy Phys. 02 (2013) 025.
[69] M. Horoi and A. Neacsu, Shell model study of using an effective field theory for disentangling several contributions to neutrinoless double-β decay, Phys. Rev. C **98**, 035502 (2018).
[70] W. Detmold and D. J. Murphy (NPLQCD Collaboration), Neutrinoless double beta decay from lattice QCD: The long-distance $\pi^- \to \pi^+ e^- e^-$ amplitude, arXiv:2004.07404.
[71] X.-Y. Tuo, X. Feng, and L.-C. Jin, Long-distance contributions to neutrinoless double beta decay $\pi^- \to \pi^+ ee$, Phys. Rev. D **100**, 094511 (2019).
[72] J. B. Albert, G. Anton, I. Badhrees, P. S. Barbeau, R. Bayerlein, D. Beck *et al.* (EXO-200 Collaboration),

Searches for double beta decay of ^{134}Xe with EXO-200, Phys. Rev. D **96**, 092001 (2017).
[73] J. Menéndez, Neutrinoless $\beta\beta$ decay mediated by the exchange of light and heavy neutrinos: The role of nuclear structure correlations, J. Phys. G **45**, 014003 (2018).
[74] Y. K. Wang, P. W. Zhao, and J. Meng, Nuclear matrix elements of neutrinoless double-β decay in the triaxial projected shell model, Phys. Rev. C **104**, 014320 (2021).
[75] L. Coraggio, A. Gargano, N. Itaco, R. Mancino, and F. Nowacki, Calculation of the neutrinoless double-β decay matrix element within the realistic shell model, Phys. Rev. C **101**, 044315 (2020).
[76] J. Hyvärinen and J. Suhonen, Nuclear matrix elements for $0\nu\beta\beta$ decays with light or heavy majorana-neutrino exchange, Phys. Rev. C **91**, 024613 (2015).
[77] D.-L. Fang, A. Faessler, and F. Šimkovic, $0\nu\beta\beta$-decay nuclear matrix element for light and heavy neutrino mass mechanisms from deformed quasiparticle random-phase approximation calculations for ^{76}Ge, ^{82}Se, ^{130}Te, ^{136}Xe, and ^{150}Nd with isospin restoration, Phys. Rev. C **97**, 045503 (2018).
[78] M. T. Mustonen and J. Engel, Large-scale calculations of the double-β decay of ^{76}**Ge**, ^{130}**Te**, ^{136}**Xe**, and ^{150}**Nd** in the deformed self-consistent Skyrme quasiparticle random-phase approximation, Phys. Rev. C **87**, 064302 (2013).
[79] J. M. Yao, L. S. Song, K. Hagino, P. Ring, and J. Meng, Systematic study of nuclear matrix elements in neutrinoless double-β decay with a beyond-mean-field covariant density functional theory, Phys. Rev. C **91**, 024316 (2015).
[80] L. S. Song, J. M. Yao, P. Ring, and J. Meng, Nuclear matrix element of neutrinoless double-β decay: Relativity and short-range correlations, Phys. Rev. C **95**, 024305 (2017).
[81] N. L. Vaquero, T. R. Rodríguez, and J. L. Egido, Shape and Pairing Fluctuation Effects on Neutrinoless Double Beta Decay Nuclear Matrix Elements, Phys. Rev. Lett. **111**, 142501 (2013).
[82] J. Yao, B. Bally, J. Engel, R. Wirth, T. Rodríguez, and H. Hergert, Ab Initio Treatment of Collective Correlations and the Neutrinoless Double Beta Decay of ^{48}Ca, Phys. Rev. Lett. **124**, 232501 (2020).
[83] A. Belley, C. Payne, S. Stroberg, T. Miyagi, and J. Holt, *Ab Initio* Neutrinoless Double-Beta Decay Matrix Elements for ^{48}Ca, ^{76}Ge, and ^{82}Se, Phys. Rev. Lett. **126**, 042502 (2021).
[84] J. Kotila and F. Iachello, Phase space factors for $\beta^+\beta^+$ decay and competing modes of double-β decay, Phys. Rev. C **87**, 024313 (2013).
[85] M. Krivoruchenko, F. Šimkovic, D. Frekers, and A. Faessler, Resonance enhancement of neutrinoless double electron capture, Nucl. Phys. **A859**, 140 (2011).
[86] J. Kotila, J. Barea, and F. Iachello, Neutrinoless double-electron capture, Phys. Rev. C **89**, 064319 (2014).
[87] F. F. Karpeshin, M. B. Trzhaskovskaya, and L. F. Vitushkin, Nonresonance shake mechanism in neutrinoless double electron capture, Phys. At. Nucl. **83**, 608 (2020).
[88] K. Blaum, S. Eliseev, F. A. Danevich, V. I. Tretyak, S. Kovalenko, M. I. Krivoruchenko, Y. N. Novikov, and J. Suhonen, Neutrinoless double-electron capture, Rev. Mod. Phys. **92**, 045007 (2020).
[89] A. Babič, D. Štefánik, M. I. Krivoruchenko, and F. Šimkovic, Bound-state double-β decay, Phys. Rev. C **98**, 065501 (2018).
[90] T. Tomoda, $0^+ \to 2^+$ $0\nu\beta\beta$ decay triggered directly by the Majorana neutrino mass, Phys. Lett. B **474**, 245 (2000).
[91] M. Duerr, M. Lindner, and K. Zuber, Consistency test of neutrinoless double beta decay with one isotope, Phys. Rev. D **84**, 093004 (2011).
[92] J. Menéndez, A. Poves, E. Caurier, and F. Nowacki, Disassembling the nuclear matrix elements of the neutrinoless $\beta\beta$ decay, Nucl. Phys. **A818**, 139 (2009).
[93] J. Barea, J. Kotila, and F. Iachello, $0\nu\beta\beta$ and $2\nu\beta\beta$ nuclear matrix elements in the interacting boson model with isospin restoration, Phys. Rev. C **91**, 034304 (2015).
[94] J. Coursey, D. Schwab, J. Tsai, and R. Dragoset, Atomic weights and isotopic compositions (version 4.1), 2015, http://physics.nist.gov/Comp [2019, 12, 12] National Institute of Standards and Technology, Gaithersburg, MD.
[95] J. C. Pati and A. Salam, Lepton number as the fourth "color", Phys. Rev. D **10**, 275 (1974).
[96] R. N. Mohapatra and J. C. Pati, "Natural" left-right symmetry, Phys. Rev. D **11**, 2558 (1975).
[97] G. Senjanovic and R. N. Mohapatra, Exact left-right symmetry and spontaneous violation of parity, Phys. Rev. D **12**, 1502 (1975).
[98] P. Duka, J. Gluza, and M. Zrałek, Quantization and renormalization of the manifest left–right symmetric model of electroweak interactions, Ann. Phys. (N.Y.) **280**, 336 (2000).
[99] W. Dekens and D. Boer, Viability of minimal left–right models with discrete symmetries, Nucl. Phys. **B889**, 727 (2014).
[100] M. Nemevsek, G. Senjanovic, and V. Tello, Connecting Dirac and Majorana Neutrino Mass Matrices in the Minimal Left-Right Symmetric Model, Phys. Rev. Lett. **110**, 151802 (2013).
[101] S. P. Martin, A supersymmetry primer, Adv. Ser. Dir. High Energy Phys. **18**, 1 (1998).
[102] M. Hirsch, H. V. Klapdor-Kleingrothaus, and S. G. Kovalenko, Supersymmetry and neutrinoless double β decay, Phys. Rev. D **53**, 1329 (1996).
[103] M. Hirsch, H. V. Klapdor-Kleingrothaus, and S. G. Kovalenko, New Constraints on R-Parity-Broken Supersymmetry from Neutrinoless Double Beta Decay, Phys. Rev. Lett. **75**, 17 (1995).
[104] H. E. Haber and G. L. Kane, The search for supersymmetry: Probing physics beyond the standard model, Phys. Rep. **117**, 75 (1985).
[105] H. P. Nilles, Supersymmetry, supergravity and particle physics, Phys. Rep. **110**, 1 (1984).
[106] P. Zyla *et al.* (Particle Data Group Collaboration), Review of particle physics, Prog. Theor. Exp. Phys. **2020**, 083C01 (2020).
[107] P. D. Bolton, F. F. Deppisch, and P. S. B. Dev, Neutrinoless double beta decay via light neutralinos in R-parity violating supersymmetry, J. High Energy Phys. 03 (2022) 152.

[108] S. Dimopoulos and L. Susskind, Mass without scalars, Nucl. Phys. **B155**, 237 (1979).
[109] B. Gripaios, Composite leptoquarks at the LHC, J. High Energy Phys. 02 (2010) 045.
[110] H. Fritzsch and P. Minkowski, Unified interactions of leptons and hadrons, Ann. Phys. (N.Y.) **93**, 193 (1975).
[111] I. Dorsner and P. Fileviez Pérez, Unification without supersymmetry: Neutrino mass, proton decay and light leptoquarks, Nucl. Phys. **B723**, 53 (2005).
[112] I. Doršner, S. Fajfer, and N. Košnik, Leptoquark mechanism of neutrino masses within the grand unification framework, Eur. Phys. J. C **77**, 417 (2017).
[113] I. Doršner, S. Fajfer, A. Greljo, J. Kamenik, and N. Košnik, Physics of leptoquarks in precision experiments and at particle colliders, Phys. Rep. **641**, 1 (2016).
[114] M. Hirsch, H. V. Klapdor-Kleingrothaus, and S. G. Kovalenko, New leptoquark mechanism of neutrinoless double β decay, Phys. Rev. D **54**, R4207 (1996).